

Inter-annual snow accumulation and meter-scale variability from trench measurements at Dome C, Antarctica

Adrien Ooms¹, Mathieu Casado¹, Ghislain Picard², Laurent Arnaud², Maria Hörhold³, Andrea Spolaor⁴, Rita Traversi⁴, Joel Savarino², Patrick Ginot², Pete Akers⁵, Birthe Twarloh³, and Valérie Masson-Delmotte¹

¹Laboratoire des Sciences du Climat et de l'Environnement, LSCE/IPSL, CEA-CNRS-UVSQ, Université Paris-Saclay, Gif sur Yvette, France

²Institut des Geosciences de l'Environnement (IGE), Université Grenoble Alpes / CNRS, UMR 5001, Grenoble, France

³Department of Geosciences, Alfred-Wegener-Institut Helmholtz-Zentrum für Polar- und Meeresforschung, Bremerhaven, Germany

⁴Institute of Polar Sciences, National Research Council of Italy (ISP-CNR), Venice, Italy

⁵Discipline of Geography, School of Natural Sciences, Trinity College Dublin, Dublin, Ireland

Correspondence: Adrien Ooms (adrien.ooms@lsce.ipsl.fr) and Mathieu Casado (mathieu.casado@lsce.ipsl.fr)

Abstract.

The central regions of the East Antarctic ice sheet contains some of the oldest ice on earth, due to low snow accumulation rates and consistently cold conditions. One consequence of low accumulation however is that the little snow amount which is deposited at irregular times is more strongly affected by erosion and re-deposition by wind, inducing local mixing and loss of snowfall events in the snowpack. This discontinuous deposition leads to highly disturbed snow layers, limiting the interpretation of climate records from ice cores in these regions to time scales larger than decades. In order to interpret climate records at higher temporal resolution it is crucial to assess and quantify the local patterns of snow accumulation leading to stratigraphic noise.

Here, we reconstruct the spatial and temporal variability of snow accumulation in Central Antarctica using chemical composition and physical properties in 35 vertical profiles sampled in a 50 m long snow trench at Dome C. We show that a high resolution alignment of the chemistry profiles is a suitable method for inter-annual dating of the single trench profiles, allowing the reconstruction of accumulation time series with a 1 year resolution over the last 20 years. This reconstruction shows annually-varying past surface configurations, with up to 10 % of the surface subject to annual accumulation hiatus. More persistent patterns with timescales of years are also evidenced, causing difference in snow age of up to 4 years at similar depth in neighboring profiles, highlighting the complex dynamics of the snow accumulation in central Antarctica.

1 Introduction

Antarctica is a key region for the global hydrological cycle due to its large reserve of fresh water, stored as ice sheets of up to 4 km in thickness (Frémand et al., 2023). Under the influence of climate change, the Antarctic ice sheet is losing mass at an overall rate of 127 Gt per year (Diener et al., 2021), and could contribute to sea level rise by up to 30 cm by the year 202100 (Intergovernmental Panel On Climate Change (IPCC), 2023). The magnitude and rate of the future mass loss remains associated with deep uncertainty (Intergovernmental Panel On Climate Change (IPCC), 2023), in particular the positive input coming from the atmosphere, referred to as the surface mass balance (SMB). In Antarctica, SMB is the net accumulation of snow and ice resulting from total precipitation, net sublimation and snow drift to the ocean. While mass loss is increasing due to the warming climate, it is partially offset by the projected increase in SMB (Hanna et al., 2024). However, it is difficult to evaluate the change of SMB in Antarctica (Ekaykin et al., 2024), in part due to the difficulty to measure accumulation rates (Magand et al., 2007), as well as the large spatial variability at scales ranging from meters (Picard et al., 2019; Hirsch et al., 2023) to kilometers (Genthon et al., 2016; Dallmayr, 2025). This local spatial variability of accumulation is due to interactions between the freshly deposited snow, and wind scouring and redeposition (Sommer et al., 2018), an ensemble of processes often referred to as *stratigraphic noise*. Stratigraphic processes are key elements of the SMB (Zuhr et al., 2021), leading to patchy deposition (Picard et al., 2019; Goodwin, 1990), appearing as self organized dunes, with shapes similar to those found in sand deserts (Poizat et al., 2024). Improvements of SMB modeling in regional climate models (Agosta et al., 2019; Wang et al., 2016; Mottram et al., 2021; van Wessem et al., 2018) requires better estimates of not only the mean SMB but also of the local spatial variability.

Several direct measurement methods are available to study accumulation and its spatial variability at the local scale, including laser scanners, photogrammetry and stake networks, with temporal resolution of hours to multiple decades (Picard et al., 2019; Genthon et al., 2016; Ekaykin et al., 2023; Zuhr et al., 2021; Sommer et al., 2018). Chemical and physical tracers can also provide stratigraphic markers in the snowpack reaching several decades in the past (Caiazzo et al., 2021; Petit et al., 1982), but their temporal resolution strongly depends on accumulation rates. Snow pit chemical stratigraphy studies can reach annual resolution at sites with relatively high accumulation rates ($> 30 \text{ cm yr}^{-1}$), such as sites in Greenland (Kjær et al., 2021), and sites of moderate accumulation rates in Antarctica ($> 10 \text{ cm yr}^{-1}$) such as South Pole (Dibb and Whitlow, 1996) and Drowning Maud Land (DML) (Hirsch et al., 2023; Münch et al., 2016). At DML, the implementation of a 2D sampling of the snowpack in the form of a trench (e.g. simultaneous sampling of snow profiles along a well defined transect), has shown to overcome the problem of stratigraphic noise and opened the possibility to derive information on deposition history of single snow layers (Laepfle et al., 2016; Münch et al., 2016). Furthermore, the link between trace elements and snow micro-structure seasonal variability has been studied (Moser et al., 2020). Studies of snow pits from Dome F (Hoshina et al., 2014; Iizuka et al., 2004), which features low snow accumulation similar to Dome C, successfully applied layer counting at 2 cm based on post-depositional seasonality of SO_4^{2-} .

In the Dome C snowpack, seasonal differences in snow cannot be resolved and therefore traditional layer counting in the physical or chemical stratigraphy is not possible (Caiazzo et al., 2021). Measurements of the chemical composition in snow

50 pits show multi-annual variability. Various sources of have been identified, including biological activity, sea salt, terrestrial dust, and anthropogenic activities (Delmas et al., 1985; Cosme et al., 2005; Caiazza et al., 2021). On this multi-annual signal are superimposed sharp exceptional markers at multi-decadal to centennial intervals, due to volcanic or nuclear test fallout. These markers serve as temporal tie points in the snow pack (Le Meur et al., 2018; Gautier et al., 2016; Petit et al., 1982), but they only offer a decadal resolution, at best. In between these tie points, dating relies on linear interpolation which overlooks
55 the strong inter-annual variability of snow accumulation rate (Genthon et al., 2016). Estimates of snow accumulation rates from the snowpack at Dome C at sub-decadal timescales are still lacking. One of the main limitations in using chemical and physical tracers in snow pits as stratigraphic markers is their high spatial variability due to stratigraphic noise (Gautier et al., 2016), which therefore requires several simultaneous snow pits to be captured.

In this work, we study the local spatial variability of accumulation rates at Dome C, using a new dataset of snow properties
60 measured in a 50 m long, 1.5 m deep snow trench dug in the 2019-2020 summer season, completed with similar measurements in older snow pits dug in the 2000-2020 period (Traversi et al., 2009; Caiazza et al., 2021; Gautier et al., 2016; Bertinetti et al., 2020). The trench contains 35 snow profiles sampled at 3 cm vertical resolution, with horizontal inter-profile spacing ranging from 30 cm to 2 m. Chemical tracers and snow properties including snow microstructure (density, specific surface area (SSA) and penetrometry) were measured. We observed that the measured sulfate and methanesulfonic acid (MSA) concentrations
65 represent a background signal that is recognizable in the entire trench. Moreover, the sulfate signal in the trench can be matched with that of older snow pits sampled in the area that overlap with the trench depth range. We combined these two observations to derive an age model for the entire trench. Based on the age model, we derive a time series of accumulation rate at the sub-decadal timescale, and its spatial variability at the decimeter to decameter scale. Finally, we compare our results to accumulation rates from atmospheric reanalysis and from direct measurement methods.

70 **2 Methods**

2.1 Sampling and measurements

At Dome C (75° 06' S, 123° 20' E.), we excavated a 50 m long and 1.5 m deep straight snow trench in which 35 vertical snow profiles were sampled over three weeks in December 2019. The trench was perpendicular to the main orientation of the wind and the sampling was carried out on the wall face sheltered from the wind, which is southerly on average at Dome C (Genthon
75 et al., 2021). Individual samples were collected directly from the wall in 12 mL Corning tubes, and the 2D horizontal and vertical coordinates of the sample were recorded. We used a laser level to establish a common reference height for all of the profiles, materialized by a horizontal string (visible in figure 1b and d). Throughout the article, we refer to the absolute depth, z , of each sample as the vertical distance to this common height reference, in contrast with the (regular) depth usually defined as the vertical distance to the local surface. The surface topography was rather flat ($50 \text{ cm} < z < 60 \text{ cm}$) in the left section of
80 the trench (0-35 m) and a 30 cm high dune (minimum $z = 20 \text{ cm}$) was present on the right section (35-50 m) (Fig. 1a). Vertical profile sampling took place every 2 horizontal meters along the whole trench and in addition finer horizontal resolutions (from 10 cm to 1 m) was applied near the left end of the trench (between 0 m and 5 m), on the ascending slope of the dune (between

38 m and 44 m), and on top of the dune near the right end of the trench (around 48 m). Along this trench, the profiles are labeled P followed by their horizontal position in meters measured from the left end of the trench. Most profiles were sampled
85 with a 3 cm vertical resolution and four profiles, P0, P0.3, P47.7 and P48, had a higher vertical resolution of 1.5 cm. P0 was replicated 30 cm to the left. Similarly, P0.3 was replicated 20 cm to the left, and P48 was replicated 30 cm to the right. Because the decorrelation length is roughly 1 m (Appendix, Fig. A5), it is possible to mix snow from profiles 10 or 30 cm away, respectively. Here, some of the snow samples of high resolution profiles did not have sufficient amount of snow to realize the entire span of chemical measurements (anions and cations), so in this case, we used extra snow from the replicate profile
90 to complement. For simplicity, we kept the labels P0, P0.3 and P48 for these composite profiles. This short horizontal spread does not impact the results as we later focus on the coarser 2 m horizontal resolution.

After sampling, the snow samples in the Corning sampling tubes were parafilmmed, and kept frozen during shipment to laboratories in Europe. The samples were analyzed by ion chromatography at the Alfred Wegener Institute (Bremhaven, Germany) and the Institut des Géosciences et de l'Environnement (Grenoble, France) for the concentration of anions (SO_4^{2-} ,
95 NO_2^- , NO_3^- , MSA, Cl^- , Br^- , oxalate, F^- , acetate and formate) and cations (Li^+ , Na^+ , NH_4^+ , K^+ , Mg^{2+} , and Ca^{2+}).

We also deployed a Snow Micro Pen (Schneebeil et al., 1999) to estimate snow hardness. This measurement was carried out after the chemical sampling, with the probe applied 20 cm behind the exposed wall of the snow trench. Measurements were realized every 25 cm along the trench (200 profiles). The vertical resolution is extremely fine (0.004 mm) but the measurements were averaged at 1 cm resolution to obtain a macroscopic significance. The snow hardness probe was set to penetrate up to
100 150 cm, but it stopped earlier for several profiles due to too hard layers, leaving a few incomplete profiles. The Snow Specific Surface Area (SSA), a measure of the grain to pore interface surface area relative to the ice mass (unit: $\text{m}^2 \text{kg}^{-1}$) was measured using ASSSAP (Arnaud et al., 2011), Libois et al. (2014). SSA was measured at 3 cm resolution along the same profiles as the chemistry samples. Snow density was measured at 3 cm resolution along the same profiles as the chemistry samples using a scale and squared metal sampler tool with a known volume.

105 The measurements carried out on each vertical profile were combined to create a 2-dimensional image for each chemical and physical tracer in the upper 1.5 m of snow (Sect. 3.1).

2.2 Inter-profile alignment

In order to derive accumulation from the snowpack, we constructed an age model for the trench. Instead of computing an age model for each profile independently, we proceed in two steps: in the alignment step (this section), we relate each depth profile
110 in the trench to the depth of a reference profile by a squeeze and stretch function. The tie points for this transformation are obtained by matching features such as peaks and crests in the signal of three selected tracers: SO_4^{2-} , methanesulfonic acid (MSA), and SSA. In the dating step (next section), we compute an age model for a single reference profile. The age model for the entire trench is then obtained by applying the transformation of the alignment step to the reference age model.

To select tie points across the pits, we developed a versatile alignment software in Python hereafter referred to as *Alice*
115 (*A*lignment interface for *i*ce cores). This software allows the user to select tie points across a variety of chemical and physical tracers. We used the three aforementioned tracers, with SO_4^{2-} chosen as the primary tracer. Sulfate SO_4^{2-} is considered as a

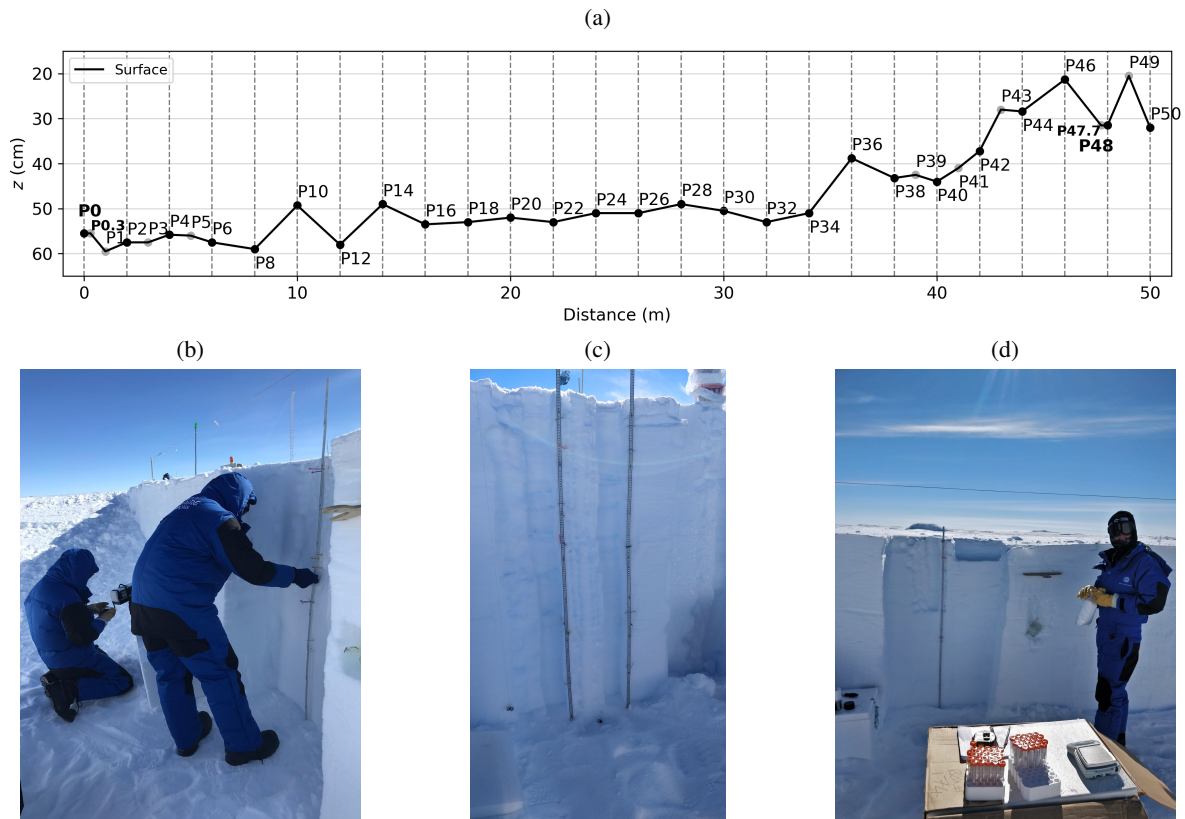


Figure 1. (a) Surface of the trench in absolute depth vertical coordinate and horizontal distribution of the profiles. Each profile is labeled as P followed by its horizontal distance to the profile P0. The vertical coordinate, absolute depth z , indicates the vertical distance to an arbitrary reference height. Profiles at 2 m spacing are displayed with black circles and constitute a subset of 26 profiles uniformly distributed along the trench. The surface is rather flat in the first 35 m, and there is a 30 cm high dune in the last 15 m. The majority of profiles is sampled at 3 cm vertical resolution. Higher resolution (1.5 cm) profiles P0, P0.3, P47.7 and P48 are highlighted with bold labels. Short horizontal bars at P0, P0.3 and P48 illustrate the horizontal sampling range for these profiles. (b,c,d) Field photographs illustrating the trench sampling operations. The reference height $z = 0$ is materialized by the horizontal string (b,d).

being preserved in snow (Wagnon et al., 1999; Traversi et al., 2009), showing only moderate peak broadening except over timescales of thousands of years, due to diffusion (Barnes et al., 2003). Using *Alice*, a profile to be aligned is viewed against a previously selected reference profile. As the trench was sampled at the beginning of summer, before significant metamorphism had occurred (Picard et al., 2012), we used the high SSA values ($> 40 \text{ m}^2\text{kg}^{-1}$) of recently deposited winter snow (Libois et al., 2015) to match the topmost portions of the profiles and to detect hiatus in snow deposition. We have performed a sensitivity test to ensure that this was also an appropriate threshold for the trench dataset. We counted all SSA values in the trench dataset (26 evenly distributed profiles) above a certain threshold, for threshold values ranging from $20 \text{ m}^2\text{kg}^{-1}$ to $60 \text{ m}^2\text{kg}^{-1}$. We see a clear transition around $38\text{--}42 \text{ m}^2\text{kg}^{-1}$, where the datapoint count increases sharply under $38 \text{ m}^2\text{kg}^{-1}$, indicating a longer

125 persistence of such SSA values during grain coarsening. This confirms that $40 \text{ m}^2\text{kg}^{-1}$ is a sweet spot to identify fresher snow (Supplements, Fig. S1). The rest of the profile is aligned by matching sulfate peaks, first with the largest peaks and then refined with sub-features. If the sulfate peak matching is ambiguous, MSA profiles were consulted. We note that MSA is well preserved in the first 100 cm depth, despite MSA disappearing at higher depth (Curran et al., 2002; Traversi et al., 2009).

We chose to use the single raw profile P0 as the reference profile because of its higher resolution (1.5 cm instead of 3 cm) and the presence of several sulfate features that are suitable as an alignment target. Despite these advantages, we observed that P0 features a lower SSA in its top snow than other profiles, and that on some profiles up to 3 cm of upper snow could not be matched to this reference. We interpret these facts as a missing snow layer at the top of P0. To solve this issue, we completed the 3 cm upper part of P0 with the mean surface snow properties in the 3 cm upper part of all profiles over the trench. This permits us to align all profiles with respect to the reference up to the surface (Supplements, Sect. S3.1). Similarly to this missing snow layer at the surface, in any single raw profile, there will be missing layers that can hinder alignment with other profiles. Yet, we chose to stick with aligning against a single reference profile because a pre-averaged profile is too smooth to obtain confidence in identifying successive peaks. We realized sensitivity tests about the impact of aligning on a single reference profile, as described in the Discussion section 4.2.

To summarize, the alignment routine goes as follows: **(1)** Display a profile to align P on top of the reference profile R leveling the top of the profiles; **(2)** looking at SSA values, evaluate whether top of the profile P contains fresh snow, or on the contrary is subject to an annual hiatus, and choose the topmost tie point (Fig. 2a and d); **(3)** align the rest of the peaks with sulfate, starting with main crests and peaks, and refining with sub-features (Fig. 2b and e). **(4)** in case of ambiguous peak matching, switch to MSA profiles to resolve uncertainties (Fig. 2c and f).

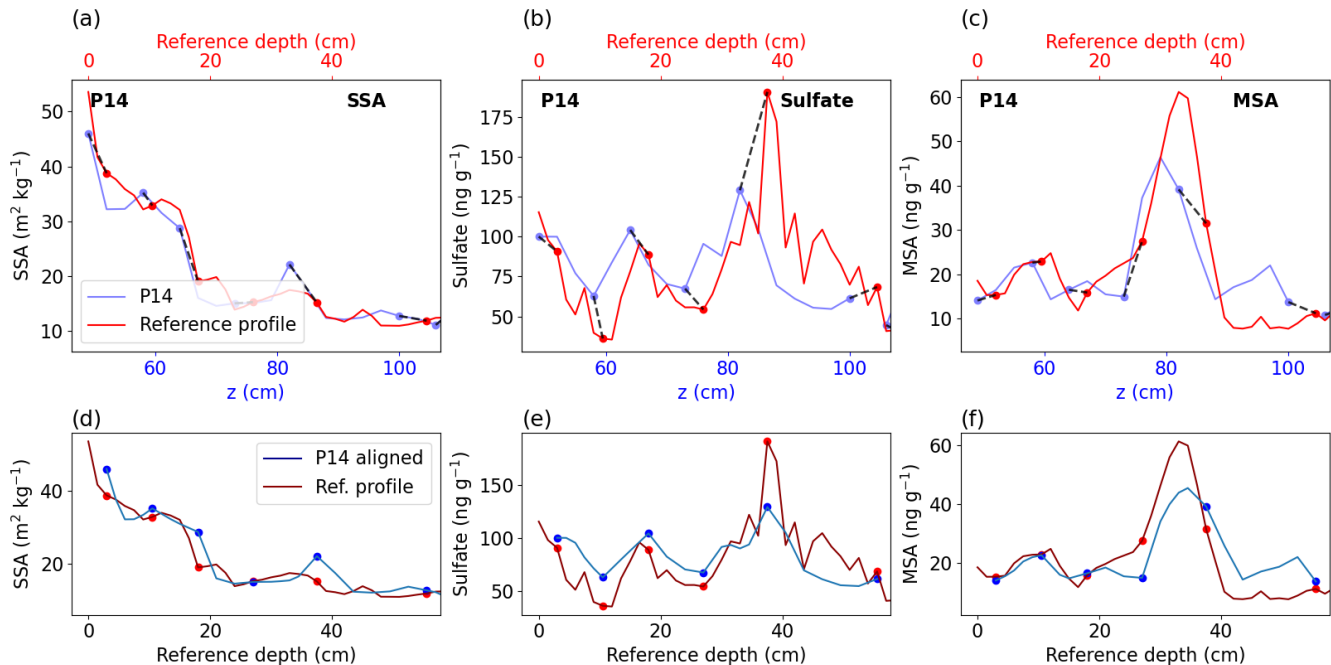


Figure 2. Example of alignment in the software *Alice*, showing SSA (a,d), sulfate (b,e) and MSA (c,f). The alignment of the topmost (50 cm) section of P14 is shown, illustrating the complementarity of the three tracers. In the upper panels (a,b,c), SSA, sulfate and MSA are shown side by side for P14 (blue) and reference profile (red) (alignment step (1)). The tie points are selected, and a preview of the aligned profiles are shown in the lower panel (d,e,f): the mid-range SSA value of $45 \text{ m}^2\text{kg}^{-1}$ on the first data point of P14 suggests that matching the head of P14 onto the second data point of the reference profile (alignment step (2)); Peaks of sulfate and MSA both support that we should match the rest of P14 slightly further right on the reference profile (alignment step (3)); the sharper drop of MSA around $z = 90 \text{ cm}$ refines the alignment on the slightly broader sulfate peak (alignment step (4)).

2.3 Dating of the reference profile

145 We construct an age model for the reference profile. This age model is then propagated to the aligned profiles in the entire
 trench. Based on previously published snow accumulation rates (8 cm yr^{-1} , Genthon et al. (2016)), we did not expect to reach
 the current depth of the Pinatubo sulfate level (about 2 m depth), deposited in Antarctica in 1992 (Cole-Dai and Mosley-
 Thompson, 1999; Caiazzo et al., 2021), so we have no volcanic horizon in the trench to serve as a dating point. Instead, our
 age model relies on similarities between the trench reference sulfate profile and sulfate concentrations in previous snow pits
 150 dug in the Dome C area in the 2000-2020 period. We were able to align these sulfate profiles together (Fig. 3) and considered
 that the top of each of these snow pits is an certain absolute dating point on the reference profile.

From the set of 22 snow pits dug at Dome C in the last 20 years (Gautier et al., 2016; Traversi et al., 2009; Caiazzo et al.,
 2021) we selected 13 that could be aligned with the reference profile of the trench (the others showed no remarkable feature in
 common with the reference in their upper 15 cm section). This $9/22 = 41 \%$ discarding ratio is comparable to the observations

155 of Gautier et al. (2016), where they showed that a volcanic peak only has 60% chance of being present in any two given cores. To construct the age model of the reference profile, we chose to only keep the top of each snow pit as an absolute tie point, as it is the date known with the highest confidence. The alignment was realized for the 13 profiles, giving 13 dating points on the reference profile. However only six dating points were kept for the age model due to several snow pits being dug within the same month, resulting in duplicate tie points (Table 1). Error bars were assigned to the tie points depth on the reference profile.

160 The error ranges between 5 and 10 cm depending on the quality of the match in sulfate signals. Small errors (5 cm) are assigned to the tie points just before a large and recognizable feature such as the broad sulfate peak in the 90-120 cm depth (December 2005), but conservative errors (10 cm) are assigned to tie points in a series of similar peaks, or in a section with little overlap, such as at depth 140-150 cm, corresponding to December 2000. For a comprehensive use of all the data, we ensured that the error bars associated with the dating capture the variability observed across these duplicates. We used a different approach to

165 obtain a dating point for the bottom of the reference, where alignment with an older snow pit is not possible due to the lack of overlap. The snow pits covering the Pinatubo horizon were associated with a linear age model between the date of sampling and 1992. This age model was then transferred to the reference after alignment (Fig. 3 (b) and (d), upper x-axis). The mean of these age models is used to get a temporal tie point for the bottom of the reference profile. The error bar in dating for this tie point is the standard deviation of tie point age among age models. Figures for the alignment of all snow pits, including

170 duplicates, are presented in the Appendix (Fig. A1).

In the dating routine, for visual aid, the snow pit to be aligned and the trench reference profile have a depth offset corresponding to the accumulated snow between times of sampling. The depth offset was calculated using 8 cm snow per year (Genthon et al., 2016).

| Sample date | Type | Max depth | Resolution | Species | Short name & reference | Pinatubo |
|-------------|----------|-----------|------------|-------------------------------------|---|----------|
| 12-2000 | snow pit | 7.3m | 2.5 cm | SO ₄ ²⁻ , MSA | Traversi2000 (Traversi et al., 2009) | x |
| 12-2005 | snow pit | 4m | 3 cm | SO ₄ ²⁻ , MSA | Traversi2005 (Traversi et al., 2009) | x |
| 1-2008 | snow pit | 3.8m | 5 cm | SO ₄ ²⁻ , MSA | Savarino2008 (Savarino, private communication) | x |
| 1-2012 | ice core | 100 m | 2-3 cm | SO ₄ ²⁻ | VolSol (Gautier et al., 2016) | x |
| 12-2017 | snow pit | 3.8 m | 3 cm | SO ₄ ²⁻ , MSA | Spolaor2017 (Spolaor et al., 2021) | x |
| 12-2017 | snow pit | 3.9 m | 3-4 cm | SO ₄ ²⁻ , MSA | Traversi2017 (Bertinetti et al., 2020) | x |
| 1-2019 | snow pit | 0.5 m | 2 cm | SO ₄ ²⁻ | DCE_IGE15 (Savarino, private communication) | |

Table 1. Summary information for the snow pits and ice cores used in the dating. Last column indicates whether the Pinatubo volcanic horizon of 1992 can be identified in the sulfate signal, allowing us to compute a linear age model for that snow pit. Only the snow pits whose upper tie-points were used for dating are shown (non duplicates, 6/13), except for Traversi2017, which is redundant, but whose linear volcanic age model is shown alongside other snow pits in Fig. 5 for validation.

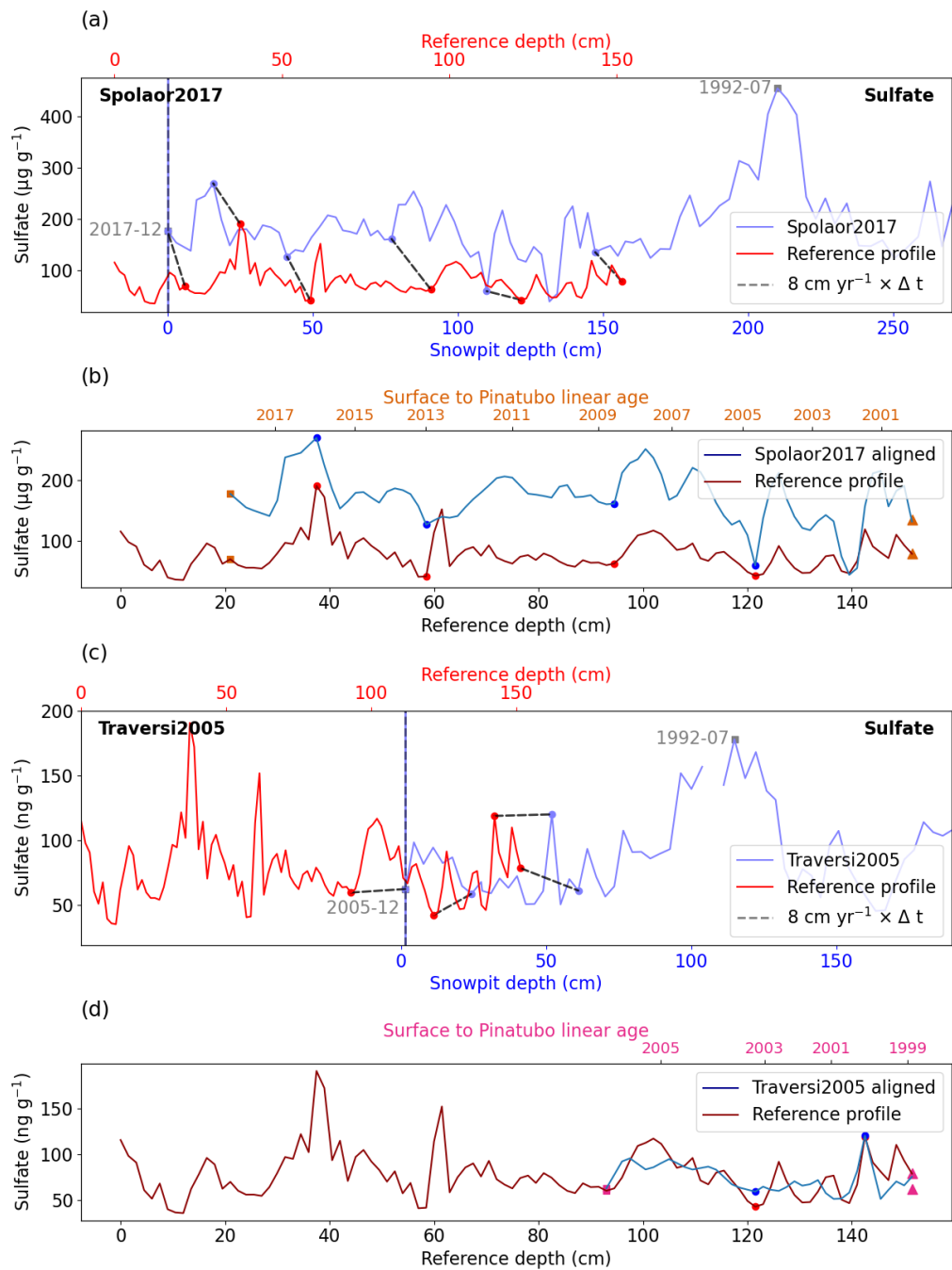


Figure 3.

Figure 3. Example of dating in the software *Alice*, showing the alignment of the reference profile with a snow pit from 2017 ("Spolaor2017") (Spolaor et al., 2021) (a,b) and snow pit from 2005 ("Traversi2005") (Traversi et al., 2009) (c,d). On the upper panels (a,c), the snow pit profile (blue) is overlaid on top of reference profile (red). An initial depth shift is applied between both profiles, corresponding to the time difference between the two sample dates multiplied by a constant elevation change rate of 8 cm snow per year. Both of these profiles show the Pinatubo eruption horizon (Spolaor2021, depth = 210 cm, Traversi2005, depth = 115 cm), assigned with a deposition date in mid-1992. The lower panel (b,d) shows the result of the alignment, with the signals displayed on the reference profile depth scale. The snow pit surface tie point, associated to the sampling date of the snow pit, together with the Pinatubo horizon, provides an age model on the reference (upper x -axis, (b,d)). Only the top tie points (orange (b) and pink (d) squares) and the mean of the bottom tie points (orange (b) and pink (d) triangles) are kept for the final age model of the reference profile.

2.4 Additional accumulation data

175 The accumulation rates we calculated in this study are compared to other available datasets. First, the changes of elevation
measured every year around Dome C since 2005 (Genthon et al., 2016) in the GLACIOCLIM stake network which can be
converted into accumulation. This network consists of 50 stakes located 2 km south to the Concordia station (75° 12' S, 123°
32' E.). The stakes are spaced approximately 40 m apart, arranged in a 1 km x 1 km cross. The stakes are measured every
year. Second, we compare our results with 3 years of high resolution accumulation data estimated from the elevation maps
180 measured by an autonomous surface laser scanner called Rugged LaserScan (RLS), which was operational from January 2015
to December 2015 (period 1) and from January 2016 to December 2017 (period 2) (Picard et al., 2016a, 2019). The timeseries
has daily resolution. The spatial setup of the instrument between both periods was different (total scanned area of 40 and 110
m² and horizontal resolution of 2 and 3 cm respectively). We only use the second period for detailed spatial analysis as its
spatial extent is closer to that of the trench, and the continuous 2 years of data are necessary to capture important features of
185 the accumulation dynamics.

The elevation change obtained from both the stake network and the laser scanner is converted into accumulation rate in mass
equivalent using constant density value. Following the literature, we use a reference surface density of 320 kg m⁻³ (Genthon
et al., 2016; Libois et al., 2015; Stefanini et al., 2025). In addition, we present the results obtained with a density of 295
kg m⁻³, which seem to be better suited according to our observations. This latter value is based on the trench density profiles
190 (Fig. A2) and on other published data reporting density around 300 kg m⁻³ (Brun et al., 2011; Champollion et al., 2019).

We also compared our results with the outputs of the fifth generation ECMWF Reanalysis (ERA5) (Hersbach et al., 2020)
estimating the accumulation as the difference between the total precipitation variable (mm w.e.) and the total evaporation and
summed over a year. The output of the reanalyses is selected at the grid point nearest Dome C (75° 00' S, 123° 25' E.). ERA5
accumulation rates shows good agreement with observations in Antarctica at the regional scale (Wang et al., 2025).

3.1 2D profiles

Sulfate concentration shows a high profile-to-profile, and intra-profile variability (Fig. 4), characterized by a mean value of 72 ng g^{-1} and a standard deviation of 20 ng g^{-1} . Global patterns of high and low concentrations are present across the trench, with small to high differences ($\pm 10\text{-}30$ cm) in absolute depth. For instance, around $z = 80$ cm, sulfate concentrations above 100 ng g^{-1} were measured in almost all profiles. Similarly, local minimum concentrations of about 50 ng g^{-1} were measured in almost all profiles around $z = 140$ cm. The deepest coherent layer which can be identified in the aligned trench, corresponding to a minimum sulfate concentration of 50 ng g^{-1} , is located around $z = 180$ cm. There were about 15 measurements on the reference profile P0 outside of the ± 1 standard deviation range, which provided a convenient target for alignment with the other profiles. We refrained from interpreting these cycles as seasonal signal, and focused on identifying global multi-annual patterns between profiles. These patterns suggest that the chemical tracers can be used to obtain tie points between the depth profiles in the trench (Sect. 2.2). From these tie points, isochrones are drawn across the trench, as represented by the gray dashed lines in Fig. 4. We assume that these isochrones are associated with past accumulation events (Gautier et al., 2016), and therefore represent past configurations of the surface topography. An inspection of the density profile against depth shows that density is about 10% lower in the upper 6 cm section of the trench compared to the full profiles (295 kgm^{-3} vs 328 kgm^{-3}), although no significant trend is found in the average density profile up to 1.5 m depth (Appendix, Fig. A2). This indicates that deformation of surface features is less than 10 % during the burial process. Note that the dating of the isochrones is carried out in Section 3.2.

The chemical tracer tie points are used to align the profiles together. The aligned trench shows an increase in inter-profile correlation ($\bar{r} = 0.3$) (Fig. S3) compared to the leveled trench ($\bar{r} = 0.1$) (Fig. A3), as expected since sulfate is used to align the trench. It is noteworthy that in horizontal averages, phase differences in the signal (phase noise) due to different deposition depths have been significantly reduced in the aligned trench compared to the leveled trench (Appendix, Fig. A3). The use of an independent proxy is necessary to validate the alignment, which is provided by snow hardness measurements (Sect. 3.2). The horizontal decorrelation length of the sulfate signal (Appendix Sect. A3) is 1.05 m (e-fold) in the leveled trench and 1.40 m in the aligned trench. This supports the use the evenly 2 m spaced out subset of profiles (Fig. 1 a, bold labels) when computing horizontal averages of tracer or accumulation rates, in order to avoid local scale correlation of the time series.

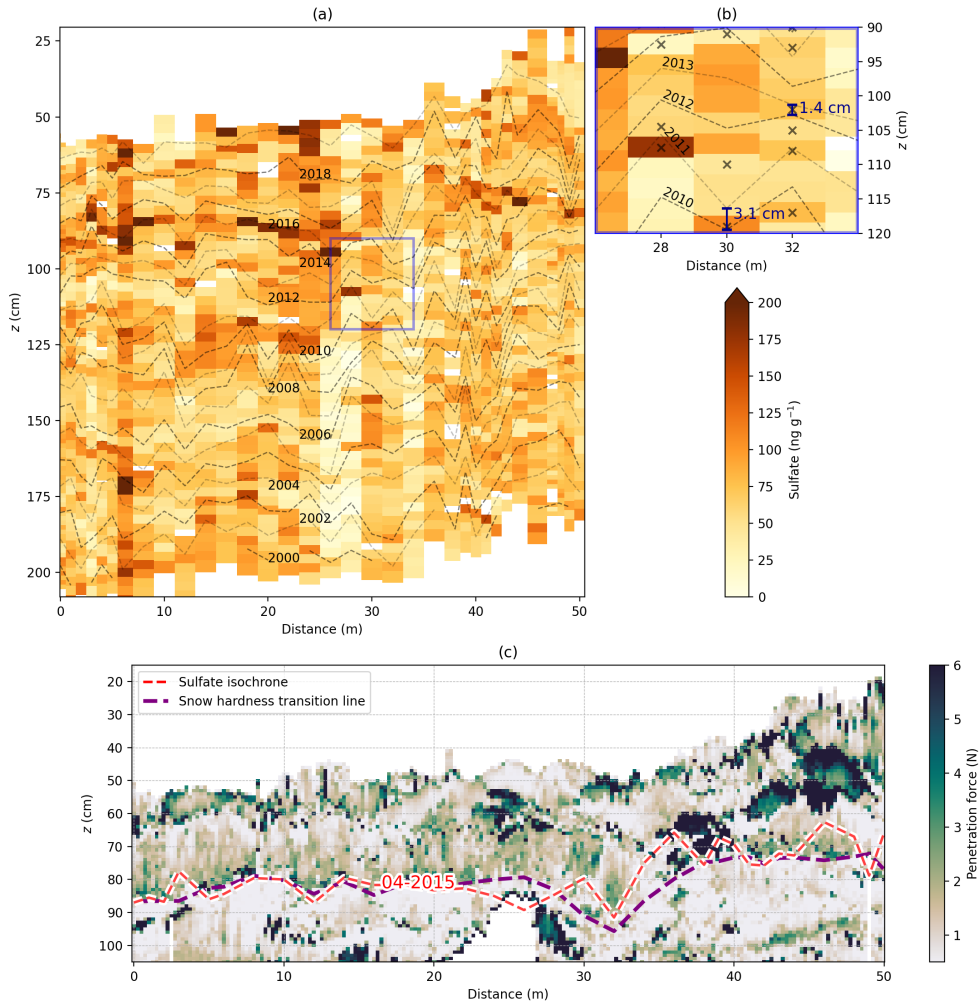


Figure 4. Dated stratigraphy obtained as a result of the alignment and dating procedure, overlaid on the sulfate concentration in the entire trench (a) and in a subset, chosen for its low accumulation (i.e. an accumulation hiatus) (b), and on the snow hardness (penetration force) in the upper section of the trench (c). Isochrones are interpreted as past surface configuration, and the depth between successive isochrones is the amount of snow accumulation in between these years. In (a), the blue rectangle indicates subset shown in (b). On (b) the zoomed in portion exhibits low accumulation (3.1 cm) at profile P30 for the year 2010, and accumulation below the 3 cm resolution threshold (1.4 cm) on P32 for the year 2012 (purple vertical segments). The tie points used for the alignment are indicated with light gray "x" signs. In (c), the dashed red line indicates the sulfate isochrone closest to a transition between soft and hard snow layers. Our age model attributes this past surface configuration to April 2015, which is contemporary to recorded extreme wind and temperature conditions of April 2015 described in Leduc-Leballeur et al. (2017) (red star, Fig. 5).

3.2 Absolute dating

The age model obtained on the P0 reference profile is shown in Fig. 5. The dating is calculated by linear extrapolation of eight temporal tie points over the depth of the reference profile as detailed in Sect. 2.3.

The first dating point is on top 1.5 cm of the reference profile, which corresponds to the most recent snow deposition before the date of sampling (December 2019), with no error, since there is no accumulation hiatus at the surface in the reference profile (Sect. S3.1).

The next six dating points were obtained by alignment of the reference profile to snow pits dug in the Dome C area over the past 20 years. The depth uncertainty of dating points (horizontal error bars in Fig. 5) leads to an uncertainty in the snow age at a given reference depth (vertical error bars) ranging from ± 0.5 years for the January 2019 tie point to ± 1.5 years for the January 2012 tie point. The average limited spread of the individual age models (dotted colored lines in Fig. 5) has an mean standard deviation of 0.7 years between models and gives confidence in the accuracy of the trench age model at ± 1 year.

The last tie point at the bottom of the reference profile is obtained from the mean over the six linear age models transferred from the aligned snow pits reaching the Pinatubo horizon (Table 1). The standard deviation among the age models gives an error estimate. They indicate that the snow layer buried at 151.5 cm depth was deposited in early 1999 ± 1 years. From the surface snow deposited in June 2019, the trench thus archives about 21 years of snow accumulation, with a mean elevation increase of 7.3 cm yr^{-1} .

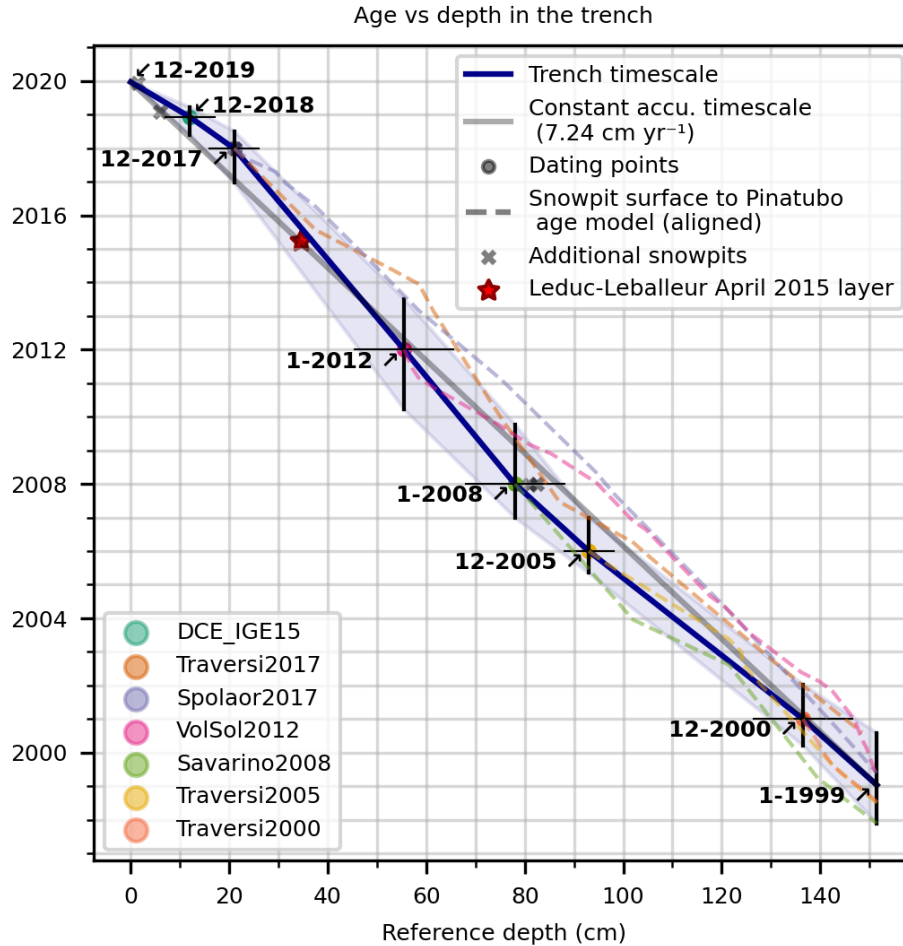


Figure 5. Age model on the reference profile: eight dating points across the 151.5 cm depth of the reference profile; 1 dating point at the surface from the sampling time of the trench, six dating points in the bulk from the alignment with snow pits dug in the 2000-2020 period at Dome C (keeping only the tie point at the surface of the snow pit), and 1 dating point at the bottom of the trench by taking the mean of the six snow pits age models. The solid blue line shows the resulting age model for the reference used for the dated stratigraphy. Horizontal error bars show the depth uncertainty for the snow pit alignment while vertical ones show the corresponding age uncertainty. Dashed lines show the age models of the snow pits, obtained by linear interpolation between the surface and the Pinatubo volcanic horizon of mid-1992, and aligned onto the reference profile (Fig. A1b (2017, orange) and d (2005, pink), upper x -axis). The solid black line is the age model computed from the bottom 1999 tie point only, equivalent to a constant accumulation on the reference profile. The accumulation that would result from such a dating is provided for comparison in the Appendix (Sect. A4).

We evaluate how closely the dated isochrones in the trench (Fig. 4a) can be interpreted as past surface topography using the SMP as an independent variable not used for the alignment. The dated isochrones drawn on top of the SMP measurements are shown in Figure 4a. We use the case of the mid-2015 isochrone as a validation of the past topography because it follows
240 closely a clear boundary between a softer and an harder layer detected by the SMP: the Pearson correlation coefficient between the hardness boundary and the isochrone is $r = 0.67$, $p < 0.05$, with only 4 cm average vertical distance between the two lines. The origin of the hard layer detected in mid 2015 is likely the signature in the snowpack of a remarkable meteorological event described in Leduc-Leballeur et al. (2017), as discussed in section 4.2.

3.3 Mean accumulation time series

In order to reconstruct accumulation, the stratigraphy based on the isochrones is combined with density measurement to convert
245 observed elevation change in cm yr^{-1} of snow into accumulation in $\text{kg m}^{-2}\text{yr}^{-1}$. The mean trench accumulation time series is calculated as the mean of the 26 profiles evenly distributed across the trench (2 m apart). The mean density measured over the trench is 328 kg m^{-3} with a standard deviation of 42 kg m^{-3} . The surface snow (depth < 6 cm) has density of $293 \pm 28 \text{ kg m}^{-3}$, 10% lower than the average. Overall, we observe no detectable densification in the first 1.5 m depth, which
250 justifies that the distance between isochrones is representative of the accumulation depth at deposition time. The mean annual accumulation of the 26 trench profiles only differs by 4% on average when using mean density of 328 kg m^{-3} compared to full density profiles in the trench, while the difference in total accumulation for the period 2001-2019 are negligible (<0.1%) when using average vs spatially resolved densities (Sect. A7). Although the reference profile age model reaches as far as early 1999, the starting year for the accumulation reconstruction is set to 2001, since is it the first year identified on all of the profiles.
255 The resulting time series is shown in Figure 6. It spans from early 2001 to late 2019 with a mean accumulation of $23.9 \pm 1.5 \text{ kg m}^{-2} \text{ yr}^{-1}$. The error is estimated as the combination of the uncertainty of the depth of the 2001 layer ($135 \pm 3 \text{ cm}$,) and the dating uncertainty around ± 1 year in 2001.

GLACIOCLIM stake network elevation change are converted to accumulation rate using a constant density value ρ_{surf} . The reference density value is $\rho_{\text{surf}} = 320 \text{ kgm}^{-3}$. Based on the density observed in the surface snow in the trench, we propose
260 a second value of density of $\rho_{\text{surf}} = 295 \text{ kgm}^{-3}$ to convert snow elevation change to accumulation rate. With a density of 320 kg m^{-3} , the accumulation rate estimate is $26.7 \pm 0.3 \text{ kg m}^{-2} \text{ yr}^{-1}$ (for 2004-2019). A density of 295 kg m^{-3} yields $24.6 \pm 0.3 \text{ kg m}^{-2} \text{ yr}^{-1}$ (for 2004-2019). The ERA5 reanalysis time series for the 2001-2019 period is $24.9 \text{ kg m}^{-2} \text{ yr}^{-1}$ precipitation and $2.6 \text{ kg m}^{-2} \text{ yr}^{-1}$ evaporation rate, resulting in $22.3 \text{ kg m}^{-2}\text{yr}^{-1}$ net accumulation rate. We note that the net accumulation from ERA5 does not include potential contribution of snow drift, contrary to the trench and stakes data.
265 Turning to spatial variability, taking $2\sigma/\sqrt{n}$ as the spatial envelope where σ is the standard deviation across profiles and n is the number of profiles, we obtain $2\sigma/\sqrt{n} = 4.5 \text{ kg m}^{-2} \text{ yr}^{-1}$ for the trench (26 profiles, 50 m scale) and $2\sigma/\sqrt{n} = 6.5 \text{ kg m}^{-2}\text{yr}^{-1}$ for GLACIOCLIM stakes (50 profiles, 1 km scale) ($5.8 \text{ kg m}^{-2}\text{yr}^{-1}$ with $\rho_{\text{surf}} = 295 \text{ kgm}^{-3}$). Finally, the inter-annual standard deviation in accumulation rates is quite comparable between the three datasets, with $4.4 \text{ kg m}^{-2} \text{ yr}^{-1}$ for the trench (2001-2019 period), $5.7 \text{ kg m}^{-2} \text{ yr}^{-1}$ for GLACIOCLIM stakes with $\rho_{\text{surf}} = 320 \text{ kgm}^{-3}$ (2004-2019 period)
270 ($5.2 \text{ kg m}^{-2}\text{yr}^{-1}$ with $\rho_{\text{surf}} = 295 \text{ kgm}^{-3}$) and $3.8 \text{ kg m}^{-2} \text{ yr}^{-1}$ for ERA5. Restricting to the 2004-2019 period does not

change the results by more than 3% for the trench and ERA5. While the amplitudes are also similar, there is a slight difference in phase (Fig. 6), which could be attributed to local spatial variability of the 50 m long trench. This point is discussed in the Appendix A5.

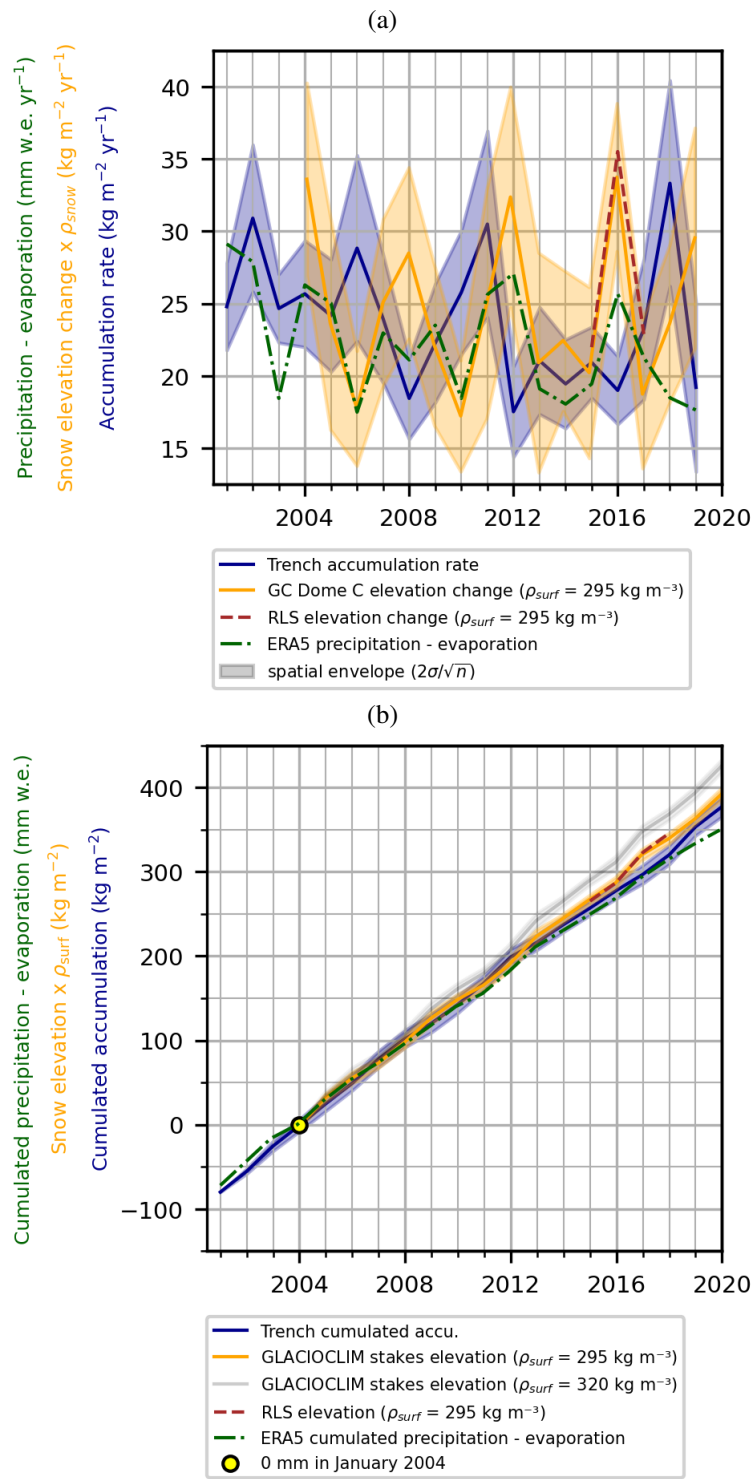


Figure 6.

Figure 6. (a) Accumulation time series. GLACIOCLIM stakes and RLS data are converted to accumulation with the constant density value of $\rho_{\text{surf}} = 295 \text{ kg m}^{-3}$. For comparison, we also show the accumulation rate of GLACIOCLIM stakes with a density of $\rho_{\text{surf}} = 320 \text{ kg m}^{-3}$. The envelopes display twice the standard deviation in the spatial component, divided by the square root of the number of profiles (50 stakes for GLACIOCLIM, 26 profiles for the trench). ERA5 accumulation is the annual total precipitation minus evaporation. The mean values of accumulation are $23.9 \text{ kg m}^{-2}\text{yr}^{-1}$ (6% accurate) for the trench, $22.3 \text{ kg m}^{-2}\text{yr}^{-1}$ for ERA5 and $24.6 \text{ kg m}^{-2}\text{yr}^{-1}$ for GLACIOCLIM stakes (1% accurate). (b) Cumulated accumulation time series. Series have been set to an initial value of 0 mm in January 2004 (first GLACIOCLIM stakes measurements), and RLS initial value is set to match GLACIOCLIM in January 2015. When overlaid, the accumulation time-series of the trench follows closely that of ERA5 (precipitation - evaporation), and that of GLACIOCLIM with $\rho_{\text{surf}} = 295 \text{ kg m}^{-3}$, showing a small deviation of less than 20 kg m^{-2} (5%) over the period 2004-2019.

3.4 Frequency of accumulation hiatus

275 Annual accumulation hiatus, near zero accumulation or erosion over a year, is frequently observed near Dome C (Genthon et al., 2016; Picard et al., 2019). We investigate whether we can detect it in the reconstructed trench accumulation. In order to describe accumulation hiatus from a final accumulation product (snow pits) in which, by definition, only strictly positive accumulation is recorded, we have extended the definition of hiatus to a snow accumulation less than 3 cm over a given period of time. This 3 cm threshold corresponds to the smallest accumulation amount we can detect with the trench resolution. For
 280 example, the 2012 and 2013 isochrones in Fig. 4b are in a very narrow range of depths (< 3 cm) around profile P32, indicating an accumulation hiatus at this location for the year 2012. We consider all pairs of isochrones and compute the fraction of profiles where hiatus are occurring. We bin average this hiatus fraction by the time period separating isochrones in each pair. The same analysis is repeated on the elevation profiles of the RLS data, with a threshold of 3 cm accumulation. The hiatus fraction as a function of time period for the trench and RLS is shown in Fig. 7. The 19 years record of accumulation in the
 285 trench, with 3 cm vertical resolution, equivalent to at least 6 months temporal resolution, is compared to the 2 years time series of the RLS (period 2) with daily resolution. There are 26 evenly distributed accumulation time series 2 m apart in the trench, compared to 110 elevation change timeseries of 1 m^2 averages of the RLS (110 m^2 scanned area).

The hiatus probability is computed for the trench isochrones at monthly resolution for periods from 6 to 36 months. We did not consider periods shorter than 6 months for the trench as it is under our resolution limit. Hiatus probability reaches 42 %
 290 at 6 months (15% standard deviation across accumulation events), and 5 % at 1 year (5 % standard deviation). We found no hiatus (0%) extending over 2 years.

For the upper section of the trench (depth < 20 cm), a second computation of hiatus statistics is possible based on SSA values. SSA is decreasing for older snow and the SSA values corresponding to snow older than 1 year can be deduced from the dated trench. We found empirically a threshold value between 35 to 37 kg m^2 for 1 year old snow. The fraction of profiles
 295 with SSA values under this threshold is 3/26 and 6/26 respectively, resulting in a annual hiatus probability of 10-20% for the year 2019, higher than the estimation with the chemistry dating. The details of this alternative approach is provided in the

Supplements (Sect. S1). The same computation with the 2 years SSA threshold value of $23 \text{ m}^2 \text{ kg}^{-1}$ yields 0 profile with 2 years accumulation hiatus, agreeing with the chemistry dating.

These results are compared against the RLS dataset. The hiatus probability is computed for daily elevation maps for all periods between 1 to 730 days. The results in the RLS area are similar with an agreement at 6 months, a marked decrease with only a slightly higher (non statistically significant) probability of hiatus in the range 6 - 18 months. No accumulation hiatus over 2 years or more are detected. There is 41 % mean hiatus probability at 6 month, with a 15% standard deviation across accumulation events, and a 10 % probability at 1 year, with a 10 % standard deviation. This is close to the $5 \pm 5 \%$ estimate in the trench, considering that the observation period is 19 years for the trench and 2 years for RLS. We note that there are 2 annual accumulation events within the 19 years of the trench record that show a 20% hiatus fraction.

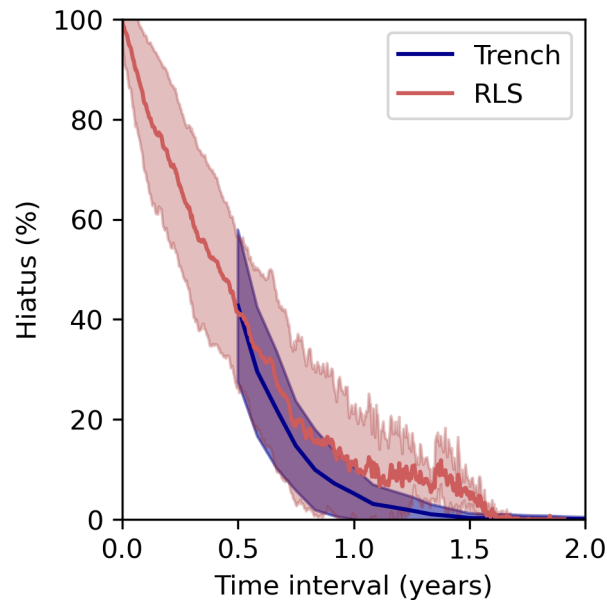


Figure 7. Probability of hiatus for a given time period in the Trench (blue) (2001-2019) and for RLS (red) (2016-2017). For a given time period, the probability of hiatus is the fraction of accumulation events with snow elevation change less than the threshold value of 3 cm (the resolution of the trench alignment). Periods shorter than 6 months are under the temporal resolution limit of the trench. The annual hiatus probability is $5 \pm 5 \%$ for the trench and $10\% \pm 10\%$ for the RLS. There are no accumulation hiatus extending beyond 2 years.

3.5 Accumulation and topography

Isochrones in Figure 4a show that the snow accumulation does not lead to a flatter surface with time, but instead the persistence of several years of some topographic features over time is observed. For instance, the 10 cm high bump around P10 took 5 years before being erased. The larger 30 cm high dune located in the 35-50 m section of the trench seems to persist throughout the accumulation record (about 20 years). We therefore hypothesize that accumulation and topography are relatively decoupled at the meter scale. In order to quantify this phenomenon, we define the following measure of local topography. At a given

point on an isochrone, we define Δz as the difference between absolute depth z of the isochrone at that point, and the mean absolute depth values of the two neighboring points (at +2 m and -2 m). Δz measures the curvature, it is negative for bumps and positive for holes.

315 Figure 8 shows the distribution of snow accumulation against Δz . While the highest accumulation amounts ($> 10 \text{ cm year}^{-1}$) are more often associated to holes as expected, the bulk of the distribution is very spread out. A linear regression gives a positive slope of 8 \% yr^{-1} , and a determination coefficient of $r^2 = 0.08$ ($p\text{-value} < 0.05$). This linear slope value of 15 \% yr^{-1} is very low compared to 100 \% yr^{-1} , the value expected for the annual filling of holes. It means that a hole on the surface (resp. bump) receives only 15% more (resp. less) annual accumulation than its surroundings. The low determination coefficient also
 320 shows that there is no consistent relationship between topography and accumulation. This supports the hypothesis of a strong multi-year persistence of the meter-scale topography.

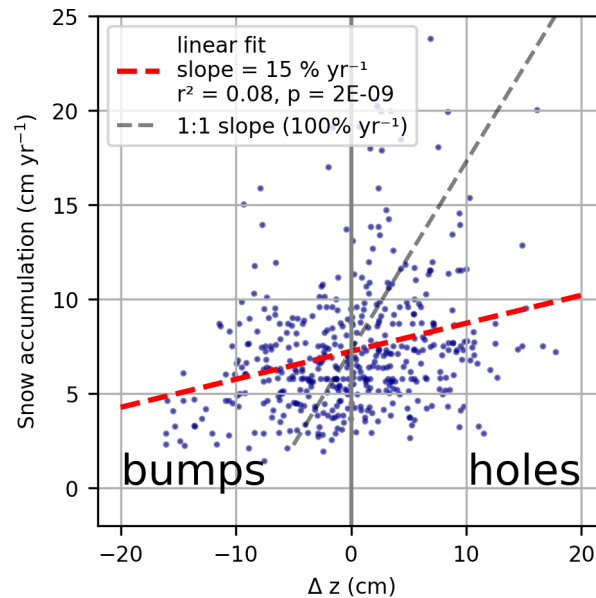


Figure 8. Correlation between annual snow accumulation and local topography anomaly Δz for the trench annual isochrones interpreted as the past surface topography. Δz measures the local curvature and is defined as the difference in absolute depth at a point compared to its direct neighbors ($\pm 2 \text{ m}$). Holes are on the positive side of the x-axis (depth greater than neighboring profiles), and bumps are on the negative side. The linear regression slope = 15 \% yr^{-1} ($r^2 = 0.08$, $p < 0.05$), red between accumulation and topography (holes accumulate more). The slope of 100 \% yr^{-1} corresponds to annual filling of the holes.

4 Discussion

4.1 Limitations of the alignment

The dated stratigraphy constructed on the trench data by inter-profile alignment and dating of the reference profile was successful in recovering sub-decadal characteristics of accumulation patterns at Dome C both in mean accumulation values, spatial and temporal variability (Sect. 3.3). However, these accumulation estimates are constrained by limitations arising from the uncertainties caused by the inter-profile alignment (Sect. 2.2), as well as the reference, single profile dating (Sect. 2.3).

One intrinsic limitation of the method is the number of recognizable features in the sulfate signal. There are about 15 peaks or crests higher or lower than the $\pm 1\sigma$ range on P0, which is reflected in the fact that 14.5 tie points per profile were used on average for the alignment, or one every 10 cm. Compared with the 21 years present in the cores, this suggests that there is no exploitable traces of seasonal variability in the sulfate signal at Dome C. This was tested by sampling four profiles at 1.5 cm resolution instead of 3 cm, namely P0, P0.3, P47.7 and P48. The average number of tie points for the 3 high resolution profiles beside the reference profile P0 was 13. This means that with 3 cm vertical resolution, we can effectively resolve the stratigraphy exploiting the full significant sulfate signal, and that the related uncertainty is effectively the precision related to sampling resolution.

The sampling resolution of 3 cm in the trench is to be compared to the annual mean accumulation of $7.8 \pm 1.4 \text{ cm yr}^{-1}$ ($23.9 \pm 4.4 \text{ kg m}^{-2} \text{ yr}^{-1}$, Sect. 3.3), meaning our precision is $3/8 = 4.5$ months on average and $3/6 = 6$ months for the thinner layers. To evaluate the impact on accumulation rate estimates, we have performed a sensitivity test on the alignment by shifting isochrones by a random height of up to 3 cm around our final alignment. The result is an uncertainty of $\pm 0.8 \text{ kg m}^{-2} \text{ yr}^{-1}$ on accumulation, or approx 3% (Sect. A4).

In addition, we estimated the global uncertainty of the dating procedure of the trench (Appendix, Fig. A1) to roughly ± 1 year, evenly affecting all profiles (Sect. 4.2). This was confirmed by the comparison between the dating of the trench and the SMP hard layer detected in March 2015, and attributed to exceptional meteorological condition around a strong wind event. The April 2015 sulfate isochrone is co-localized within 4 cm vertical distance with a boundary between higher and lower snow hardness (Fig. 4c). Leduc-Leballeur et al. (2017) documented a remarkable meteorological event in March 2015, when wind exceeding 7 ms^{-1} removed about 2 cm of fresh snow from the surface. This type of high wind speed would typically lead to harden crust, therefore the 2015 snow hardness transition could be the signature of this event. Another independent validation arises from the isotopic composition measurements where the maximum $\delta^{18}\text{O}$ values identified in the trench in summer 2014 can be found in surface snow isotopic composition time series in January 2014 and minimum values of d-excess identified in the trench in summer 2015 can be found in surface snow isotopic composition time series in January 2015 (Casado et al., 2021). Overall, we conclude that the trench stratigraphy gives local accumulation with a 6 months inter-profile resolution, and ± 1 year global uncertainty.

Beyond the temporal resolution limits of this method, we also cannot obtain negative accumulation by studying the final accumulation product in the snowpack. By contrast, the GLACIOCLIM stakes network exhibits negative annual accumulation values for 10% of the stake measurements. While negative accumulation is out of reach with the trench approach, we inves-

tigated low accumulation years (near hiatus) and found similar statistics for low accumulation events (< 3 cm) between the trench and RLS datasets (Sect. 3.4). Here again, we show that our accumulation estimates are reliable when considering layers representing at least 6 months of accumulation.

4.2 Reference profile and limitation of dating

360 We have chosen to work with a reference profile as a target for the alignment of all the profiles in the trench, instead of pair
by pair alignment. Beyond the obvious gain in time in the alignment (n vs $n(n-1)/2$ pairs to align, where $n = 35$ is the
number of profiles) and dating (only one profile to date), we also gain in coherence as all features recognizable on the reference
were matched precisely. For the same reason, we chose to work with a single raw reference profile instead of a trench stack.
Indeed, the reference profile is used as a target for the dating relative to older snow pits, which are mostly single, non-replicated
365 profiles. Stacking the trench unaligned profile produces a smooth profile (Appendix, Fig A3) which becomes unpractical for
peak matching with older snow pits. By using a single raw profile, we were unable to match 9 out of the 22 snow pits used
for dating (due to the anomalies in the reference and in the snow pits themselves), but we keep a high confidence for successful
identification of the remaining 13 snow pits. This 60% ratio is consistent with the two ice-core volcanic peak identification
rate of Gautier et al. (2016). Reference profile alignment however comes with some caveats, and the dating of the reference
370 remains the main source of uncertainty.

First, the reference profile can itself be subject to hiatus. In section 3.4, we found that annual accumulation hiatus occurs
in 5% of the profiles on average, and 6 monthly hiatus about 40% of the time. Comparing the sulfate records in five 100 m
long ice cores, Gautier et al. (2016) found a probability of 30% of missing one single volcanic event in a single core, which
is consistent considering most of the deposition takes place over less than a year Cole-Dai and Mosley-Thompson (1999).
375 Accumulation hiatus on the reference profile lead to missing minima or maxima in its sulfate record. Such a missing feature
would be present in 95% of the trench profiles and inaccurately aligned on the reference. However, with our approach, these
effects are automatically corrected for on average. For instance, if year 2015 was missing in the reference, but years 2014
and 2016 were clearly identified, the accumulation for 2014-2015 and 2015-2016 may be inaccurate, but the accumulation of
the two years period 2014-2016 would still be correct. Sensitivity tests on the choice of reference profile, using P48 instead
380 of P0 as an alignment target, indeed show such variations, changing the intensity or phasing of inter-annual accumulation
within a $5 \text{ kg m}^{-2} \text{ yr}^{-1}$ error bar. Similarly, user induced variability of inter-annual accumulation reconstruction using the
same reference, which will inevitably impact assignment of ambiguous features, is contained within a $5 \text{ kg m}^{-2} \text{ yr}^{-1}$ error bar
(Sect. A4). We have considered the alternative of using a stacked profile as the reference to get a more representative average
sulfate profile, but precisely because of stratigraphic noise, this produces a very smooth profile (Appendix, Figure A3.a) on
385 which it becomes impossible to recognize any feature at the inter-annual scale.

Second, the uncertainty of dating of the reference profile must also be considered. When aligning the reference to older
snow pits, we estimated a typical error of ± 5 cm in the depth associated to the top of the snow pit which propagates into
 ± 1 yr in the age depth scale of the stratigraphy (Sect. 3.2). We have performed a sensitivity test with variations in the age
model of the reference with ± 1 yr variations, and found variations in accumulation as high as $5 \text{ kg m}^{-2} \text{ yr}^{-1}$, i.e. about 20%

390 in individual annual accumulation rates. (Sect. A4). The uncertainty on the total accumulation of the 19 years record is 6%
(Sect. 3.3). Previous studies of snow accumulation rates have used seasonal signal in chemical tracers, in particular sulfate, to
resolve annual layers. This has been successfully applied to higher accumulation sites such as DML (Moser et al., 2020) as
well as low accumulation sites such as Dome F (Iizuka et al., 2004; Hoshina et al., 2014). Layer counting is based on sulfate
peaks observed in austral summer due to the biogenic activity (Cosme et al., 2005). We have not tried this approach in the
395 present study, as it is not applicable to our coarse resolution (3 cm). The higher resolution (1.5 cm) profiles P0 and P48 do
exhibit high frequency seesaw variability with very variable amplitude, but peak counting results in 15-25 peaks depending on
counting strategy, and it is unclear whether it could be interpreted as annual layers.

To test the sensitivity of the reference profile, we performed another alignment and dating procedure with the profile P48,
and the results are presented in the Appendix. This alternative reference alters the accumulation reconstruction at the annual
400 scale, with discrepancies of the same order as those resulting from the 20% dating uncertainty. The mean accumulation in the
period 2001-2019 is within the error bars of the first alignment using P0, and the overall shape of the mean accumulation time
series is also conserved (e.g. high value around 2012, low value around 2009, low values for 2014-2016, Fig. A3). Therefore,
we argue that, within conservative error values on the dating alone, our alignment method yields a robust and reproducible
accumulation reconstruction that is able to capture its inter-annual variability with good accuracy.

405 4.3 Comparison of accumulation time series

Different accumulation time series based on the trench and other lines of evidence (Sect. 3.3) differ slightly in mean values and
inter-annual variability, but overall agree within ranges of uncertainties.

The mean accumulation rates are $23.9 \pm 4.5 \text{ kg m}^{-2} \text{ yr}^{-1}$ (mean value for the period \pm spatial envelopes) with a 6% un-
certainty for the trench (2001-2019) and $22.9 \text{ kg m}^{-2} \text{ yr}^{-1}$ for ERA5 (3.3). The lower value of ERA5 is just within the 6%
410 uncertainty of the trench snow accumulation rate. The mean accumulation is $24.6 \pm 6.0 \text{ kg m}^{-2} \text{ yr}^{-1}$ (with a 1% uncertainty)
for GLACIOCLIM stakes (2004-2019) with the surface density $\rho_{\text{surf}} = 295 \text{ kg m}^{-3}$, or $26.7 \pm 6.5 \text{ kg m}^{-2} \text{ yr}^{-1}$ with $\rho_{\text{surf}} =$
 320 kg m^{-3} . The conversion of GLACIOCLIM stakes elevation to accumulation rate relies on the choice of a constant density,
traditionally set as $\rho_{\text{surf}} = 320 \text{ kg m}^{-3}$ (Genthon et al., 2016; Libois et al., 2015), which considers a linear regression over a 5
m density profile. Other studies recommend a density for surface snow of 300 kg m^{-3} instead (Brun et al., 2011; Champollion
415 et al., 2019). This is more in line with the direct measurements of surface density or of the value measured in the trench of
 295 kg m^{-3} (depth < 6 cm). This lower value of surface density removes the 10% gap that would otherwise arise between
GLACIOCLIM stakes and trench snow accumulation rates (Fig 6b). The reason for the overestimation of surface density could
be due to metamorphism of surface snow upon burial in the firn. Lighter snow only constitutes the superficial 5-10 cm layer
effectively considered by the stake readings, and a linear regression over more than a meter depth will over-estimate this lower
420 surface density. We note that the mean density in the trench in the depth range 0-1.5 m is 328 kg m^{-3} , and a linear regression on
the 1.5 m gives a surface density value of 320 kg m^{-3} which agrees with the density profile of Genthon et al. (2016) (Appendix,
Fig. A2).

We note that Stefanini et al. (2025) found a mean elevation change of $7.3 \pm 0.2 \text{ cm yr}^{-1}$ for the 2011-2023 period, using a stake farm of 13 poles situated 800 m south-west of Dome C, which is closer to the trench site than the GLACIOCLIM stake farm by about 1 km. This is equivalent to $23.4 \pm 0.6 \text{ kg m}^{-2} \text{ yr}^{-1}$ with $\rho_{\text{surf}} = 320 \text{ kgm}^{-3}$ and $21.5 \pm 0.6 \text{ kg m}^{-2} \text{ yr}^{-1}$ with $\rho_{\text{surf}} = 295 \text{ kgm}^{-3}$. The mean accumulation rate in the trench is $22.4 \text{ kg m}^{-2} \text{ yr}^{-1}$ for the period (2011-2019), 6 % accurate, which would be in agreement with the stake farm with either values of ρ_{surf} .

In addition, the trench accumulation rate lies within the spatial envelope of the GLACIOCLIM stakes network with either value of ρ_{surf} as the GLACIOCLIM stakes cover a 1 km x 1 km. Discrepancies due to decameter-scale variability of snow deposition needs to be taken into account, and the 50-m long trench could be a specifically low accumulation area at Dome C.

We compare the amplitudes of mean annual accumulation time series between the trench and the GLACIOCLIM stakes. The maximums displayed by the trench accumulation time series have an amplitude comparable to the maximum annual values documented by direct measurement methods and reanalysis data. The peaks however are out of phase by ± 1 year for the year 2011, and ± 2 years for 2006 and 2008 (Fig. 6). This could be due to errors in the dating of the trench chemical stratigraphy, which brings uncertainties of the order of ± 1 year. However, such dephasing of ± 1 year is observed within the GLACIOCLIM network itself (for the 2009 or 2013 peaks for instance), when considering stakes at the opposite sides of the 1 km x 1 km cross (Fig. A4). Therefore we cannot rule out that the differences in phase are not due to the intrinsic spatial variability of accumulation at km scale, as the sites of the stake farm and the trench are approximately 2 km apart.

Overall, having multiple trenches at and around Dome C would be necessary to be able to separate the spatial variability at the different scales (decimetric to kilometric) which seems to affect snow accumulation. Alternatively, simultaneous sampling of snow-pits at the same location and spatial scales as existing stake farms would allow to re-do the comparison presented here factoring out the dependency in spatial scales.

4.4 Hiatus, dune and impact on ice-cores

Laepplé et al. (2016) suggests that more than 90% of the isotopic signal archived in ice cores is noise, suggesting that it is necessary to average more than 10 ice cores 5 to 10 m apart is necessary to retrieve a coherent local isotopic signal in interior sites in Antarctica (Münch et al., 2016), and minimize noise due to accumulation variability. We evaluate the impact of accumulation variability on sub-decadal reconstruction from ice-cores drilled at Dome C. We have showed that the 30 cm dune observed in the 35-50 m section of the trench is persistent over 20 years. Taking two profiles from the trench as an example of two ice-cores drilled several meters apart, sitting on top of different configurations of past dunes, we see that they would have a depth offset of up to 30 cm that propagates over more than a 20 year long section of the cores. We quantify the age difference that snow samples at the same depth could have for this pair of hypothetical ice cores. Computing the distribution of years at a given depth based on our trench age model, the 98% quantile is 3.4 years. With our high resolution alignment, this mismatch is reduced to ± 6 month. (Sect. 4.2).

For multi-decadal or centennial records of longer ice-cores dug at Dome C, traditional alignment relies on major volcanic peaks horizons giving tie points every 50 years on average (Castellano et al., 2005). Our approach suggests that this volcanic peak matching can be taken as a preliminary alignment, and be further refined within 50 year windows using background

sulfate signal. Barnes et al. (2006) have applied a similar peak matching method to electrical conductivity profiles in replicate EDC cores, with a correlation based automatic match routine, and have found 6600 tie points for a 44 ky record, or one tie point every 7 years on average. Our work suggest that the precision could reach one tie point every 1.5 years on average by analyzing the detailed chemistry record and potentially improving automatic matching routine to reach the accuracy of manual matching. Concerning high resolution dating, while there will be no additional dating point to further refine the dating beyond volcanic horizons, as was done here with the 20 years snow pit dataset, we have showed that simple linear interpolation of the accumulation rate produces a timescale within the ± 1 year uncertainty. By combining 2 or more replicate cores at high resolution, this open the way of interpreting climatic signal in Dome C ice-core at higher frequencies, potentially reaching annual resolution.

5 Conclusions

Here, we reconstructed the last two decades of snow accumulation at Dome C at annual time scales, by using chemical composition and physical properties of 26 vertical profiles across a transect of 50 m. The mean local accumulation rate matches the ones obtained in ERA5 (total precipitation - evaporation), and from a stake farm (GLACIOCLIM, within the spatial variability). The reconstructed accumulation time series shows further similarities with observations, including inter-annual variations that can reach up to 50 % of the total local accumulation, and around 5-10% chances of annual accumulation hiatus at the profile scale.

We evaluated the spatial variability of the accumulation at the meter scale. We found that variations of 20 % in the accumulation rate along the transect on average, with a decorrelation length of roughly 1.4 meters. These statistics confirm that snowfalls are not uniformly deposited at Dome C, but instead each event forms patches of accumulation. This impacts ice core signal interpretation and contributes to the stratigraphic noise. We argue that for timescale larger than two years, the impact of these random erosion on accumulation is largely mitigated.

We observed the persistence of a 30 cm dune over the 20 years duration of the trench record. We also found that the holes in the local surface topography are filled only slightly more than the bumps (+15 % at the annual scale) leading to persistence of the topography over many years. This shows that meter scale topographic features may persists over decades of accumulation. Better understanding of the competing processes leading to the spatial pattern of the surface mass balance are key, as the detection of the influence of climate change on precipitation amounts in Polar Regions remains to be determined. In particular, dating ice cores which is often using volcanic eruptions only happening every several decades could suffer from uncertainties of a few years. Yet, our results show that the linear approximation of the age scale between tie points separated by a few decades is only leading to uncertainties of 1.5 years. This is an encouraging perspective for transposing our approach to the broader study of replicate cores covering longer time scales, where only linear interpolation between multi-decadal time horizons are available.

Appendix A

A1 More details on the dating procedure

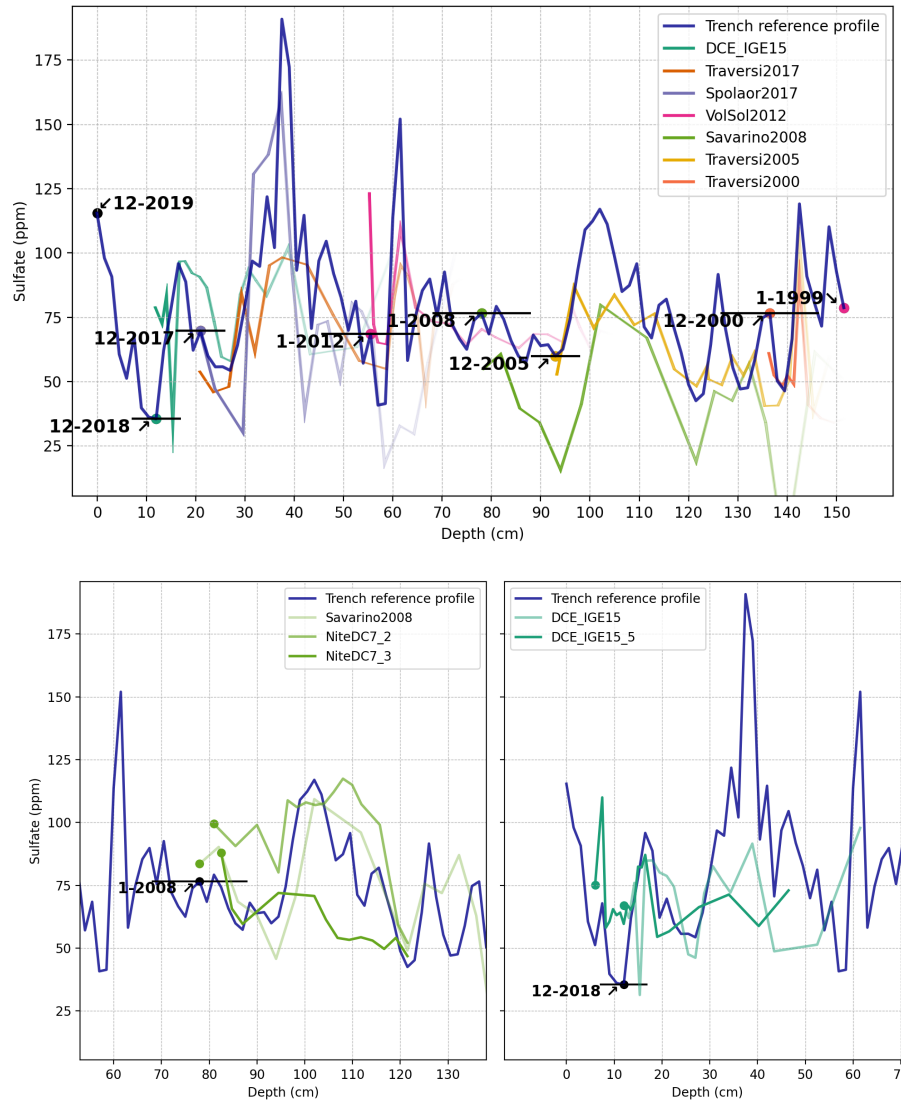


Figure A1. Illustration of the method for dating; the 6 snow pits profiles aligned with the reference. The fading on shows the first 30 cm for each profile. Bottom: two cases with duplicate snow pits for the sampling times. Different shapes for the top of the snow pits lead to variation on the corresponding depth on the reference profiles. The deviations are captured by the error bar

490 A2 Surface snow density

In our results section, we are comparing accumulation timeseries obtained from the trench data, which takes into account the density measurements in the trench, to accumulation timeseries obtained from RLS and stake farm measurements, computed from elevation change, multiplied by a constant surface snow density.

This density is often taken as 320 kgm^{-3} in the literature Genthon et al. (2016). We propose another value of 295 kgm^{-3} based on density measurements in the trench (Figure A2). While the density profile shows a very small increasing trend with depth (slope = 11 kgm^{-4}) that indeed has an intercept at 320 kgm^{-3} , the mean density in the 0-6 cm depth near the surface, which is the range where elevation change measurements take place, is only 297 kgm^{-3} . While it cannot be excluded that this is due to inter-annual variability of snow density (there is another density minimum at 30 cm depth), we observe that reconstructed accumulation rates of RLS and GLACIOCLIM are more consistent with the trench with the lower surface snow density value.

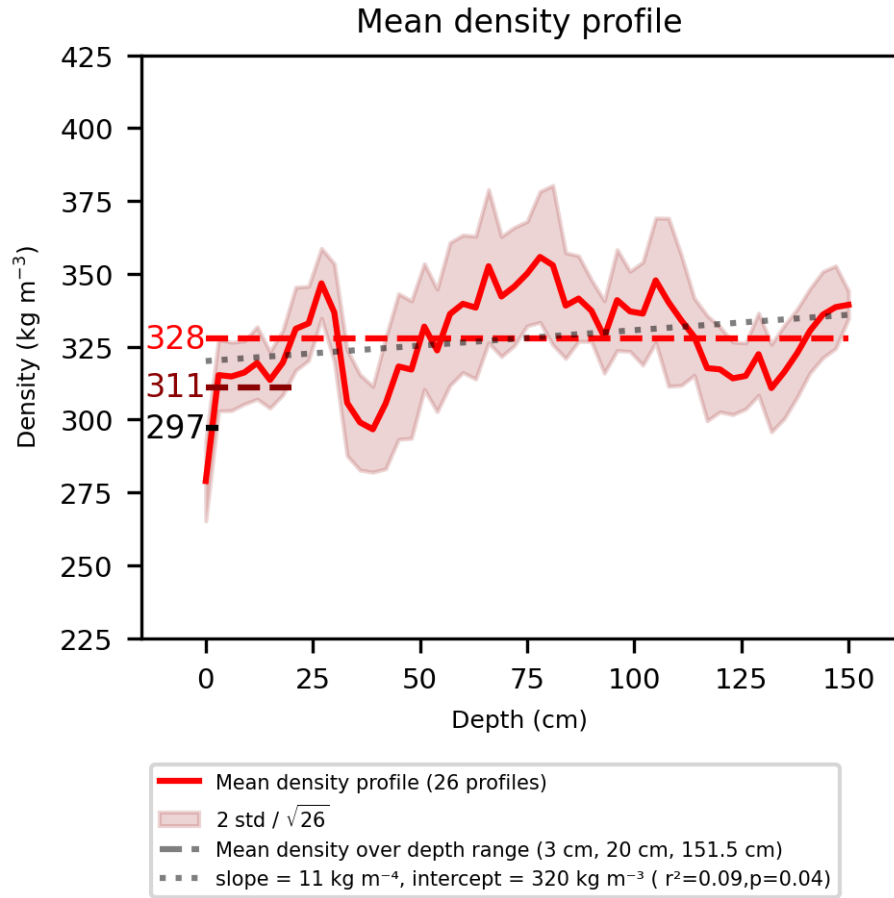


Figure A2. Mean density profile as a function of depth for the 26 evenly spaced out trench profiles. There is a high spatial variability, with only minor densification trend in the upper 1.5 m. We note that a linear regression gives a surface density of 320 kg m^{-3} as in Genthon et al. (2016). However the surface snow (0-6 cm) in the trench is about 10% lower on average, at 295 kg m^{-3} . We compare both surface density values in the manuscript to reconstruct accumulation rates from stakes measurements. The stakes accumulation rates are more consistent with trench accumulation rates when using the lower surface snow density of 295 kg m^{-3} .

A3 Supplementary figures for the evaluation of the alignment

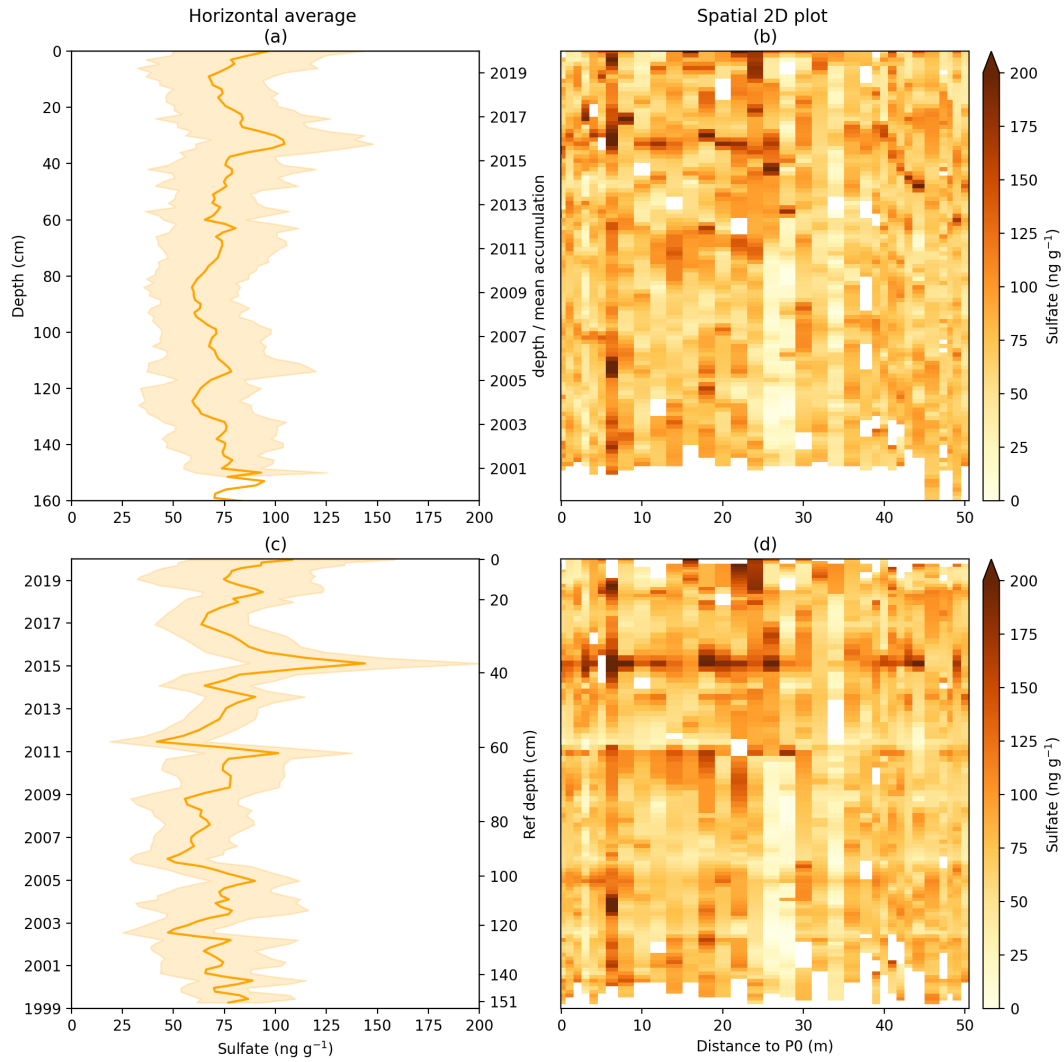
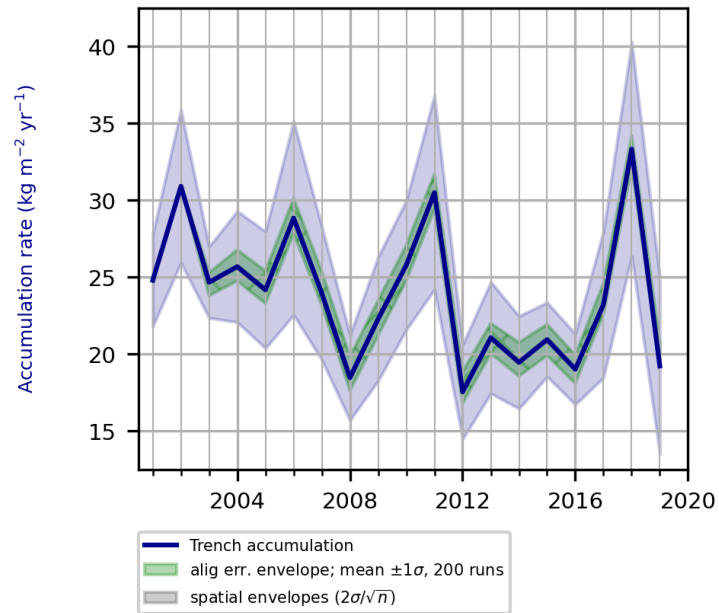


Figure A3. Effect of the alignment on horizontal averages of sulfate profiles in the trench. On top, sulfate profiles are given the simplest possible vertical alignment by setting the elevation of the surface to zero across the entire trench. At the bottom, the common vertical scale is that resulting from the alignment. Envelope indicates $2\sigma/\sqrt{n}$ for the spatial standard deviation, while the solid curve represents the mean. Secondary y -axes on the right both figures show: on top the linear time-scale that would result from constant accumulation of 8 cm yr^{-1} , at the bottom the depth scale is that of the reference profile (Sect. 2.2).

A4 Sensitivity tests for dating and alignment

(a)



(b)

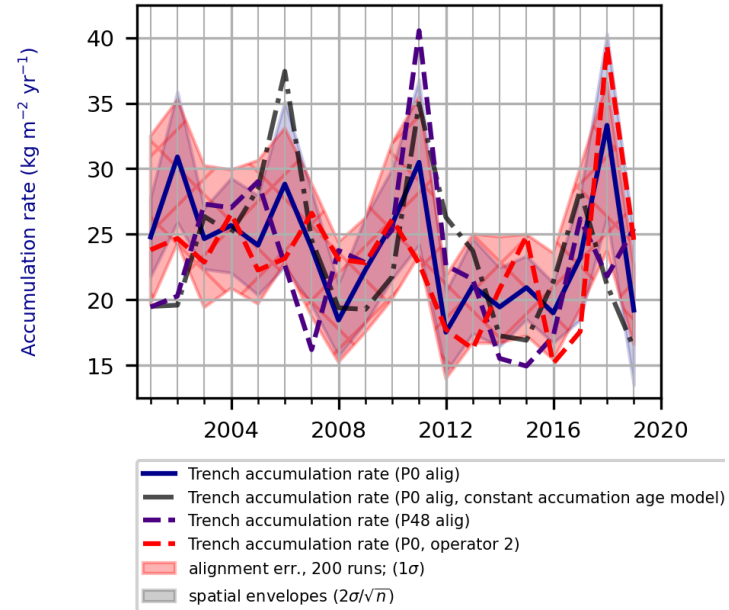


Figure A3. Sensitivity tests on the alignment and dating. [top], Montecarlo experiment with accumulation computation from isochrones modified by a uniform random variable of width ± 3 cm at each point (the alignment resolution) (200 runs). The envelope of all runs represents a standard deviation of $0.8 \text{ kg m}^{-2} \text{ yr}^{-1}$. [bottom] Montecarlo experiment where the age model on the reference profile is changed at each point by a uniform random variable of width ± 1 year. (200 runs). The envelope of all runs represents a standard deviation of $5 \text{ kg m}^{-2} \text{ yr}^{-1}$. The dashed blue line represents the accumulation reconstructed from an independent alignment and dating performed with P48 as a reference profile. Although differences are not negligible, we see that they fall within the range of the dating sensitivity test around the P0 alignment. The dashed black line is the accumulation reconstructed with a linear dating on the reference. Again it is within the range of the sensitivity test.

A5 Multi-annual accumulation dephasing

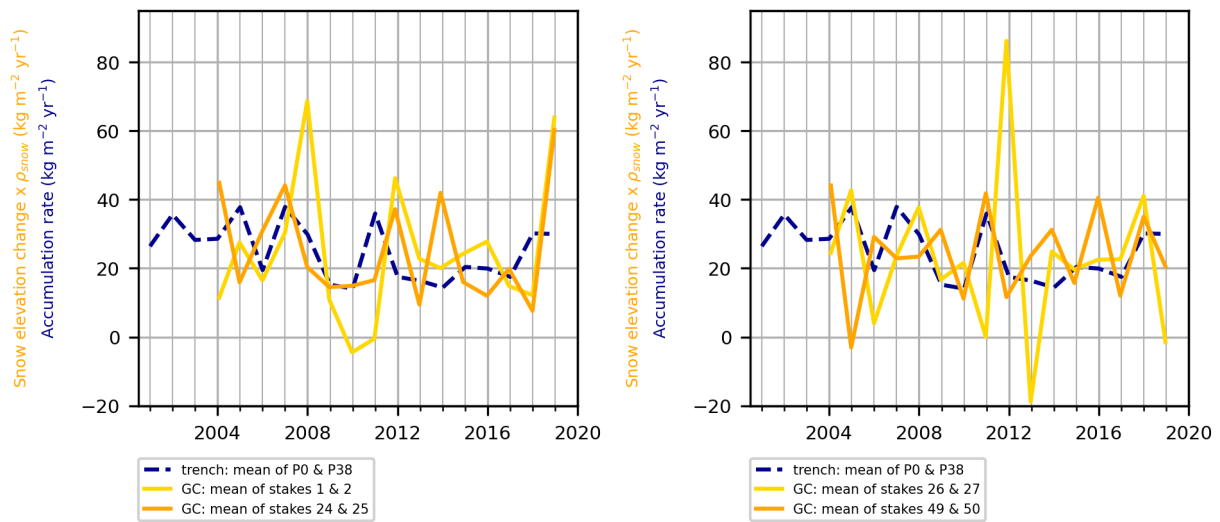


Figure A4. Mean accumulation time series of P0 et P38 compared against mean accumulation time series of four pairs of stakes approx. 40 m apart picked in glacioclim. We see that the phase mismatch of accumulation peaks is also present inside of the GLACIOCLIM stakes network itself, and we can find pairs of stakes (49 and 50) that have a maximum in 2011 just like the trench. Therefore there is a possibility that the phase mismatch in the mean accumulation time series of the paper is just a matter of spatial variability and contribution of km scale snowdrift on the snow accumulation.

A6 Spatial decorrelation of sulfate

505 We address the question of the decorrelation length of the sulfate signal. We want to extract a subset of profiles on which accumulation is free of neighbour to neighbour correlation of local noise. We compute the decorrelation length of the sulfate signal in the aligned trench. We find an e-folding / decorrelation length of 1.3m (Fig. A5). Therefore, we choose to work on the subset of 26 profiles that are evenly spaced out, located every 2 m inside the trench.

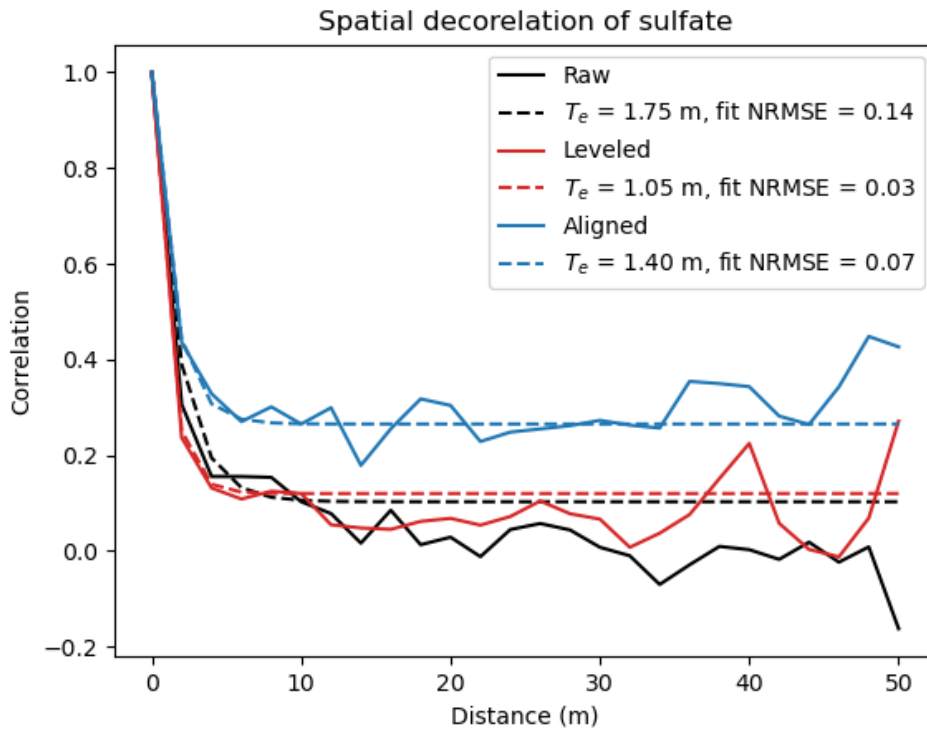


Figure A5. Spatial decorrelation of sulfate in the raw, leveled and aligned trench. We see the increase in mean value of inter-profile correlation at long distance from 0.1 to 0.3 in the aligned trench. We also see the horizontal decrease in correlation with 1.3 m e-folding. This supports the choice of the 2 m pits subset for spatial diagnosis on alignment and snow accumulation rates.

A7 Computation of accumulation for the trench

510 To get snow accumulation time series from the dated isochrones we have obtained as a result of the alignment and dating of
the trench, we must convert elevation change computed from the height difference of the isochrones, to snow accumulation
rate. We could do this with a mean density value as in the case of the RLS and stake farm data. However, to capture spatial
variability as finely as possible, we exploit the 3 cm resolution density data available for all the profiles in the trench, and
compute accumulation rate based of the density integrated between two isochrones. An illustration of this computation, is
515 given in Fig. A6. We also provide a comparison with the accumulation rate based on a constant density.

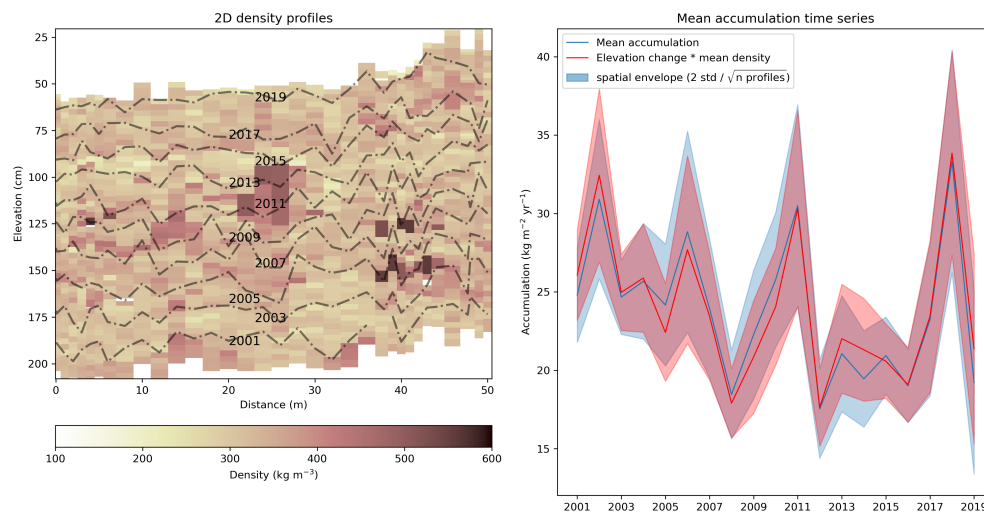


Figure A6. (left) Computation of the accumulation rate from the chemistry isochrones and the density measurement in the trench. Total snow accumulation is the density integrated between two isochrones. (right) Comparison of the accumulation time series obtained from the fully resolved density measurements and from a constant density of 328 kg m^{-3} . There is very little difference in the mean accumulation rates of the 26 profiles. This supports the use of a constant density for GLACIOCLIM stakes.

Data availability. The raw data files for the chemical composition and snow properties of all profiles and tie-points needed to reproduce the analyses of this study are available at <https://doi.org/10.5281/zenodo.18300845>

Code and data availability. The interface used for the alignment was coded using the python tkinter library for graphical interfaces. It was designed to be easy to install and to use, and applicable to any ice core data, from shallow snow pit to over 100 m deep cores. We wish that this code can help colleagues working on similar firn core or ice core alignment studies. It is available as the python package *lscealice* in the pypi.org database and can be installed as an executable python app on Windows, Mac or Linux distributions. For more information, visit the reference page at <https://pypi.org/project/lscealice/>.

Author contributions. CRediT author statement; **Adrien Ooms:** Conceptualization, Formal analysis, Visualization, Data curation, Writing - Original draft preparation, Validation, Software. **Mathieu Casado:** Project Administration, Funding acquisition, Conceptualization, Visualization, Data curation, Writing - Original draft preparation, Validation, Resources. **Ghislain Picard:** Writing - Original draft preparation, Visualization, Investigation, Data Curation, Supervision, Methodology, Resources. **Laurent Arnaud:** Writing - Original draft preparation, Visualization, Investigation, Data Curation, Supervision, Methodology. **Maria Hörold:** Resources, Data Curation. **Andrea Spolaor:** Re-

sources. **Rita Traversi**: Resources. **Joel Savarino**: Resources. **Patrick Ginot**: Resources, Data Curation. **Pete Akers**: Resources. **Birthe Twarloh**: Resources, Data Curation. **Valérie Masson-Delmotte**: Conceptualization, Supervision. **All authors**: Writing - Review & Editing. 530 Ressources: Mathieu Casado, Ghislain Picard and Pete Akers participated in field work. Patrick Ginot, Maria Hörold and Birthe Twarloh performed the chromatography measurements for the trench data. Andrea Spolaor, Rita Traversi and Joel Savarino cummunicated unpublished snow pit data used for the reference profile dating.

Competing interests. The authors declare that they have no conflict of interest.

Acknowledgements. We acknowledge the French Polar Institute (IPEV) through the program 1110 (NIVO) and 1177 (CAPOXI 35–75). This 535 research was made possible from funding from the DFG project CLIMAIC, the ERC Project SAMIR (HORIZON: European Research Council, grant no. 101116660), the Antarctic Science Bursary (project DATETRENCH), and the ANR project ANR-15-IDEX-02 for supporting data acquisition at Concordia station and laboratory analysis.

References

- Agosta, C., Amory, C., Kittel, C., Orsi, A., Favier, V., Gallée, H., van den Broeke, M. R., Lenaerts, J. T. M., van Wessem, J. M., van de Berg, W. J., and Fettweis, X.: Estimation of the Antarctic Surface Mass Balance Using the Regional Climate Model MAR (1979–2015) and Identification of Dominant Processes, *The Cryosphere*, 13, 281–296, <https://doi.org/10.5194/tc-13-281-2019>, 2019.
- Arnaud, L., Picard, G., Champollion, N., Domine, F., Gallet, J. C., Lefebvre, E., Fily, M., and Barnola, J. M.: Measurement of Vertical Profiles of Snow Specific Surface Area with a 1 Cm Resolution Using Infrared Reflectance: Instrument Description and Validation, *Journal of Glaciology*, 57, 17–29, <https://doi.org/10.3189/002214311795306664>, 2011.
- 545 Barnes, P. R. F., Wolff, E. W., Mader, H. M., Udisti, R., Castellano, E., and Röthlisberger, R.: Evolution of Chemical Peak Shapes in the Dome C, Antarctica, Ice Core: EVOLUTION OF CHEMICAL PEAK SHAPES, *Journal of Geophysical Research: Atmospheres*, 108, n/a–n/a, <https://doi.org/10.1029/2002JD002538>, 2003.
- Barnes, P. R. F., Wolff, E. W., and Mulvaney, R.: A 44 Kyr Paleoroughness Record of the Antarctic Surface, *Journal of Geophysical Research*, 111, D03 102, <https://doi.org/10.1029/2005JD006349>, 2006.
- 550 Bertinetti, S., Ardini, F., Vecchio, M. A., Caiazza, L., and Grotti, M.: Isotopic Analysis of Snow from Dome C Indicates Changes in the Source of Atmospheric Lead over the Last Fifty Years in East Antarctica, *Chemosphere*, 255, 126 858, <https://doi.org/10.1016/j.chemosphere.2020.126858>, 2020.
- Brun, E., Six, D., Picard, G., Vionnet, V., Arnaud, L., Bazile, E., Boone, A., Bouchard, A., Genthon, C., Guidard, V., Moigne, P. L., Rabier, F., and Seity, Y.: Snow/Atmosphere Coupled Simulation at Dome C, Antarctica, *Journal of Glaciology*, 57, 721–736, <https://doi.org/10.3189/002214311797409794>, 2011.
- 555 Caiazza, L., Becagli, S., Bertinetti, S., Grotti, M., Nava, S., Severi, M., and Traversi, R.: High Resolution Chemical Stratigraphies of Atmospheric Depositions from a 4 m Depth Snow Pit at Dome C (East Antarctica), *Atmosphere*, 12, 909, <https://doi.org/10.3390/atmos12070909>, 2021.
- Casado, M., Landais, A., Picard, G., Arnaud, L., Dreossi, G., Stenni, B., and Prié, F.: Water Isotopic Signature of Surface Snow Metamorphism in Antarctica, *Geophysical Research Letters*, 48, <https://doi.org/10.1029/2021GL093382>, 2021.
- 560 Castellano, E., Becagli, S., Hansson, M., Hutterli, M., Petit, J. R., Rampino, M. R., Severi, M., Steffensen, J. P., Traversi, R., and Udisti, R.: Holocene Volcanic History as Recorded in the Sulfate Stratigraphy of the European Project for Ice Coring in Antarctica Dome C (EDC96) Ice Core, *Journal of Geophysical Research: Atmospheres*, 110, <https://doi.org/10.1029/2004JD005259>, 2005.
- Champollion, N., Picard, G., Arnaud, L., Lefebvre, É., Macelloni, G., Rémy, F., and Fily, M.: Marked Decrease in the Near-Surface Snow Density Retrieved by AMSR-E Satellite at Dome C, Antarctica, between 2002 and 2011, *The Cryosphere*, 13, 1215–1232, <https://doi.org/10.5194/tc-13-1215-2019>, 2019.
- 565 Cole-Dai, J. and Mosley-Thompson, E.: The Pinatubo Eruption in South Pole Snow and Its Potential Value to Ice-Core Paleovolcanic Records, *Annals of Glaciology*, 29, 99–105, <https://doi.org/10.3189/172756499781821319>, 1999.
- Cosme, E., Hourdin, F., Genthon, C., and Martinerie, P.: Origin of Dimethylsulfide, Non-Sea-Salt Sulfate, and Methanesulfonic Acid in Eastern Antarctica, *Journal of Geophysical Research: Atmospheres*, 110, <https://doi.org/10.1029/2004JD004881>, 2005.
- 570 Curran, M. A. J., Palmer, A. S., van Ommen, T. D., Morgan, V. I., Phillips, K. L., McMorrow, A. J., and Mayewski, P. A.: Post-Depositional Movement of Methanesulphonic Acid at Law Dome, Antarctica, and the Influence of Accumulation Rate, *Annals of Glaciology*, 35, 333–339, <https://doi.org/10.3189/172756402781816528>, 2002.

- Dallmayr, R.: Topographic Effect Creates Non-Climatic Variations in Ice-Core Based Temperature Records of the Last Millennium in Dronning Maud Land, Antarctica, 2025.
- 575 Delmas, R. J., Legrand, M., Aristarain, A. J., and Zanolini, F.: Volcanic Deposits in Antarctic Snow and Ice, *Journal of Geophysical Research: Atmospheres*, 90, 12 901–12 920, <https://doi.org/10.1029/JD090iD07p12901>, 1985.
- Dibb, J. E. and Whitlow, S. I.: Recent Climate Anomalies and Their Impact on Snow Chemistry at South Pole, 1987-1994, *Geophysical Research Letters*, 23, 1115–1118, <https://doi.org/10.1029/96GL01039>, 1996.
- 580 Diener, T., Sasgen, I., Agosta, C., Fürst, J. J., Braun, M. H., Konrad, H., and Fettweis, X.: Acceleration of Dynamic Ice Loss in Antarctica From Satellite Gravimetry, *Frontiers in Earth Science*, 9, <https://doi.org/10.3389/feart.2021.741789>, 2021.
- Ekaykin, A. A., Lipenkov, V. Y., and Tebenkova, N. A.: Fifty Years of Instrumental Surface Mass Balance Observations at Vostok Station, Central Antarctica, *Journal of Glaciology*, pp. 1–13, <https://doi.org/10.1017/jog.2023.53>, 2023.
- Ekaykin, A. A., Veres, A. N., and Wang, Y.: Recent Increase in the Surface Mass Balance in Central East Antarctica Is Unprecedented for the Last 2000 Years, *Communications Earth & Environment*, 5, 1–8, <https://doi.org/10.1038/s43247-024-01355-1>, 2024.
- 585 Frémand, A. C., Fretwell, P., Bodart, J. A., Pritchard, H. D., Aitken, A., Bamber, J. L., Bell, R., Bianchi, C., Bingham, R. G., Blankenship, D. D., Casassa, G., Catania, G., Christianson, K., Conway, H., Corr, H. F. J., Cui, X., Damaske, D., Damm, V., Drews, R., Eagles, G., Eisen, O., Eisermann, H., Ferraccioli, F., Field, E., Forsberg, R., Franke, S., Fujita, S., Gim, Y., Goel, V., Gogineni, S. P., Greenbaum, J., Hills, B., Hindmarsh, R. C. A., Hoffman, A. O., Holmlund, P., Holschuh, N., Holt, J. W., Horlings, A. N., Humbert, A., Jacobel, R. W., Jansen, D., Jenkins, A., Jokat, W., Jordan, T., King, E., Kohler, J., Krabill, W., Kusk Gillespie, M., Langley, K., Lee, J., Leitchenkov, G., Leuschen, C., Luyendyk, B., MacGregor, J., MacKie, E., Matsuoka, K., Morlighem, M., Mouginit, J., Nitsche, F. O., Nogi, Y., Nost, O. A., Paden, J., Pattyn, F., Popov, S. V., Rignot, E., Rippin, D. M., Rivera, A., Roberts, J., Ross, N., Ruppel, A., Schroeder, D. M., Siegert, M. J., Smith, A. M., Steinhage, D., Studinger, M., Sun, B., Tabacco, I., Tinto, K., Urbini, S., Vaughan, D., Welch, B. C., Wilson, D. S., Young, D. A., and Zirizzotti, A.: Antarctic Bedmap Data: Findable, Accessible, Interoperable, and Reusable (FAIR) Sharing of 60 Years of Ice Bed, Surface, and Thickness Data, *Earth System Science Data*, 15, 2695–2710, <https://doi.org/10.5194/essd-15-2695-2023>, 2023.
- 590 Gautier, E., Savarino, J., Erbland, J., Lanciki, A., and Possenti, P.: Variability of Sulfate Signal in Ice Core Records Based on Five Replicate Cores, *Climate of the Past*, 12, 103–113, <https://doi.org/10.5194/cp-12-103-2016>, 2016.
- Gelaro, R., McCarty, W., Suárez, M. J., Todling, R., Molod, A., Takacs, L., Randles, C. A., Darmenov, A., Bosilovich, M. G., Reichle, R., Wargan, K., Coy, L., Cullather, R., Draper, C., Akella, S., Buchard, V., Conaty, A., da Silva, A. M., Gu, W., Kim, G.-K., Koster, R., Lucchesi, R., Merkova, D., Nielsen, J. E., Partyka, G., Pawson, S., Putman, W., Rienecker, M., Schubert, S. D., Sienkiewicz, M., and Zhao, B.: The Modern-Era Retrospective Analysis for Research and Applications, Version 2 (MERRA-2), *Journal of Climate*, 30, 5419–5454, <https://doi.org/10.1175/JCLI-D-16-0758.1>, 2017.
- 600 Genthon, C., Six, D., Scarchilli, C., Ciardini, V., and Frezzotti, M.: Meteorological and Snow Accumulation Gradients across Dome C, East Antarctic Plateau: METEOROLOGICAL AND SNOW ACCUMULATION GRADIENTS AT DOME C, *International Journal of Climatology*, 36, 455–466, <https://doi.org/10.1002/joc.4362>, 2016.
- Genthon, C., Veron, D., Vignon, E., Six, D., Dufresne, J.-L., Madeleine, J.-B., Sultan, E., and Forget, F.: 10 Years of Temperature and Wind Observation on a 45 m Tower at Dome C, East Antarctic Plateau, *Earth System Science Data*, 13, 5731–5746, <https://doi.org/10.5194/essd-13-5731-2021>, 2021.
- Goodwin, I. D.: Snow Accumulation and Surface Topography in the Katabatic Zone of Eastern Wilkes Land, Antarctica, *Antarctic Science*, 2, 235–242, <https://doi.org/10.1017/S0954102090000323>, 1990.
- 610

- Hanna, E., Topál, D., Box, J. E., Buzzard, S., Christie, F. D. W., Hvidberg, C., Morlighem, M., De Santis, L., Silvano, A., Colleoni, F., Sasgen, I., Banwell, A. F., van den Broeke, M. R., DeConto, R., De Rydt, J., Goelzer, H., Gossart, A., Gudmundsson, G. H., Lindbäck, K., Miles, B., Mottram, R., Pattyn, F., Reese, R., Rignot, E., Srivastava, A., Sun, S., Toller, J., Tuckett, P. A., and Ultee, L.: Short- and Long-Term Variability of the Antarctic and Greenland Ice Sheets, *Nature Reviews Earth & Environment*, 5, 193–210, <https://doi.org/10.1038/s43017-023-00509-7>, 2024.
- 615
- Hersbach, H., Bell, B., Berrisford, P., Hirahara, S., Horányi, A., Muñoz-Sabater, J., Nicolas, J., Peubey, C., Radu, R., Schepers, D., Simmons, A., Soci, C., Abdalla, S., Abellan, X., Balsamo, G., Bechtold, P., Biavati, G., Bidlot, J., Bonavita, M., De Chiara, G., Dahlgren, P., Dee, D., Diamantakis, M., Dragani, R., Flemming, J., Forbes, R., Fuentes, M., Geer, A., Haimberger, L., Healy, S., Hogan, R. J., Hólm, E., Janisková, M., Keeley, S., Laloyaux, P., Lopez, P., Lupu, C., Radnoti, G., de Rosnay, P., Rozum, I., Vamborg, F., Villaume, S., and Thépaut, J.-N.: The ERA5 Global Reanalysis, *Quarterly Journal of the Royal Meteorological Society*, 146, 1999–2049, <https://doi.org/10.1002/qj.3803>, 2020.
- 620
- Hirsch, N., Zuhr, A., Münch, T., Hörhold, M., Freitag, J., Dallmayr, R., and Laepple, T.: Stratigraphic Noise and Its Potential Drivers across the Plateau of Dronning Maud Land, East Antarctica, *The Cryosphere*, 17, 4207–4221, <https://doi.org/10.5194/tc-17-4207-2023>, 2023.
- Hoshina, Y., Fujita, K., Nakazawa, F., Iizuka, Y., Miyake, T., Hirabayashi, M., Kuramoto, T., Fujita, S., and Motoyama, H.: Effect of Accumulation Rate on Water Stable Isotopes of Near-Surface Snow in Inland Antarctica, *Journal of Geophysical Research: Atmospheres*, 119, 274–283, <https://doi.org/10.1002/2013JD020771>, 2014.
- 625
- Iizuka, Y., Fujii, Y., Hirasawa, N., Suzuki, T., Motoyama, H., Furukawa, T., and Hondoh, T.: SO4²⁻ Minimum in Summer Snow Layer at Dome Fuji, Antarctica, and the Probable Mechanism, *Journal of Geophysical Research: Atmospheres*, 109, <https://doi.org/10.1029/2003JD004138>, 2004.
- 630
- Intergovernmental Panel On Climate Change (IPCC): *Climate Change 2021 – The Physical Science Basis: Working Group I Contribution to the Sixth Assessment Report of the Intergovernmental Panel on Climate Change*, Cambridge University Press, 1 edn., ISBN 978-1-00-915789-6, <https://doi.org/10.1017/9781009157896>, 2023.
- Kjær, H. A., Lolk Hauge, L., Simonsen, M., Yoldi, Z., Koldtoft, I., Hörhold, M., Freitag, J., Kipfstuhl, S., Svensson, A., and Vallelonga, P.: A Portable Lightweight in Situ Analysis (LISA) Box for Ice and Snow Analysis, *The Cryosphere*, 15, 3719–3730, <https://doi.org/10.5194/tc-15-3719-2021>, 2021.
- 635
- Laepple, T., Hörhold, M., Münch, T., Freitag, J., Wegner, A., and Kipfstuhl, S.: Layering of Surface Snow and Firn at Kohnen Station, Antarctica: Noise or Seasonal Signal?, *Journal of Geophysical Research: Earth Surface*, 121, 1849–1860, <https://doi.org/10.1002/2016JF003919>, 2016.
- Le Meur, E., Magand, O., Arnaud, L., Fily, M., Frezzotti, M., Cavitte, M., Mulvaney, R., and Urbini, S.: Spatial and Temporal Distributions of Surface Mass Balance between Concordia and Vostok Stations, Antarctica, from Combined Radar and Ice Core Data: First Results and Detailed Error Analysis, *The Cryosphere*, 12, 1831–1850, <https://doi.org/10.5194/tc-12-1831-2018>, 2018.
- 640
- Leduc-Leballeur, M., Picard, G., Macelloni, G., Arnaud, L., Brogioni, M., Mialon, A., and Kerr, Y.: Influence of Snow Surface Properties on L-band Brightness Temperature at Dome C, Antarctica, *Remote Sensing of Environment*, 199, 427–436, <https://doi.org/10.1016/j.rse.2017.07.035>, 2017.
- 645
- Libois, Q., Picard, G., Arnaud, L., Morin, S., and Brun, E.: Modeling the Impact of Snow Drift on the Decameter-Scale Variability of Snow Properties on the Antarctic Plateau, *Journal of Geophysical Research: Atmospheres*, 119, 11,662–11,681, <https://doi.org/10.1002/2014JD022361>, 2014.

- Libois, Q., Picard, G., Arnaud, L., Dumont, M., Lafaysse, M., Morin, S., and Lefebvre, E.: Summertime Evolution of Snow Specific Surface Area Close to the Surface on the Antarctic Plateau, *The Cryosphere*, 9, 2383–2398, <https://doi.org/10.5194/tc-9-2383-2015>, 2015.
- 650 Magand, O., Genthon, C., Fily, M., Krinner, G., Picard, G., Frezzotti, M., and Ekaykin, A. A.: An Up-to-Date Quality-Controlled Surface Mass Balance Data Set for the 90°–180°E Antarctica Sector and 1950–2005 Period, *Journal of Geophysical Research: Atmospheres*, 112, <https://doi.org/10.1029/2006JD007691>, 2007.
- Moser, D. E., Hörhold, M., Kipfstuhl, S., and Freitag, J.: Microstructure of Snow and Its Link to Trace Elements and Isotopic Composition at Kohlen Station, Dronning Maud Land, Antarctica, *Frontiers in Earth Science*, 8, 2020.
- 655 Mottram, R., Hansen, N., Kittel, C., van Wessem, J. M., Agosta, C., Amory, C., Boberg, F., van de Berg, W. J., Fettweis, X., Gosart, A., van Lipzig, N. P. M., van Meijgaard, E., Orr, A., Phillips, T., Webster, S., Simonsen, S. B., and Souverijns, N.: What Is the Surface Mass Balance of Antarctica? An Intercomparison of Regional Climate Model Estimates, *The Cryosphere*, 15, 3751–3784, <https://doi.org/10.5194/tc-15-3751-2021>, 2021.
- Münch, T., Kipfstuhl, S., Freitag, J., Meyer, H., and Laepple, T.: Regional Climate Signal vs. Local Noise: A Two-Dimensional View of Water
660 Isotopes in Antarctic Firn at Kohlen Station, Dronning MaudLand, *Climate of the Past*, 12, 1565–1581, <https://doi.org/10.5194/cp-12-1565-2016>, 2016.
- Petit, J. R., Jouzel, J., Pourchet, M., and Merlivat, L.: A Detailed Study of Snow Accumulation and Stable Isotope Content in Dome C (Antarctica), *Journal of Geophysical Research: Oceans*, 87, 4301–4308, <https://doi.org/10.1029/JC087iC06p04301>, 1982.
- Picard, G., Domine, F., Krinner, G., Arnaud, L., and Lefebvre, E.: Inhibition of the Positive Snow-Albedo Feedback by Precipitation in
665 Interior Antarctica, *Nature Climate Change*, 2, 795–798, <https://doi.org/10.1038/nclimate1590>, 2012.
- Picard, G., Arnaud, L., Panel, J.-M., and Morin, S.: Design of a Scanning Laser Meter for Monitoring the Spatio-Temporevolution of Snow Depth and Its Application in the Alps and in Antarctica, *The Cryosphere*, 10, 1495–1511, <https://doi.org/10.5194/tc-10-1495-2016>, 2016a.
- Picard, G., Libois, Q., Arnaud, L., Verin, G., and Dumont, M.: Development and Calibration of an Automatic Spectral Albedometer to Estimate Near-Surface Snow SSA Time Series, *The Cryosphere*, 10, 1297–1316, <https://doi.org/10.5194/tc-10-1297-2016>, 2016b.
- 670 Picard, G., Arnaud, L., Caneill, R., Lefebvre, E., and Lamare, M.: Observation of the Process of Snow Accumulation on the Antarctic Plateau by Time Lapse Laser Scanning, *The Cryosphere*, 13, 1983–1999, <https://doi.org/10.5194/tc-13-1983-2019>, 2019.
- Poizat, M., Picard, G., Arnaud, L., Narteau, C., Amory, C., and Brun, F.: Widespread Longitudinal Snow Dunes in Antarctica Shaped by Sintering, *Nature Geoscience*, 17, 889–895, <https://doi.org/10.1038/s41561-024-01506-1>, 2024.
- Savarino, J.: Private Communication, 2024.
- 675 Schneebeli, M., Pielmeier, C., and Johnson, J. B.: Measuring Snow Microstructure and Hardness Using a High Resolution Penetrometer, *Cold Regions Science and Technology*, 30, 101–114, [https://doi.org/10.1016/S0165-232X\(99\)00030-0](https://doi.org/10.1016/S0165-232X(99)00030-0), 1999.
- Sommer, C. G., Wever, N., Fierz, C., and Lehning, M.: Investigation of a Wind-Packing Event in Queen Maud Land, Antarctica, *The Cryosphere*, 12, 2923–2939, <https://doi.org/10.5194/tc-12-2923-2018>, 2018.
- Spolaor, A., Burgay, F., Fernandez, R. P., Turetta, C., Cuevas, C. A., Kim, K., Kinnison, D. E., Lamarque, J.-F., de Blasi, F., Barbaro, E.,
680 Corella, J. P., Vallelonga, P., Frezzotti, M., Barbante, C., and Saiz-Lopez, A.: Antarctic Ozone Hole Modifies Iodine Geochemistry on the Antarctic Plateau, *Nature Communications*, 12, 5836, <https://doi.org/10.1038/s41467-021-26109-x>, 2021.
- Stefanini, C., Stenni, B., Masiol, M., Dreossi, G., Favier, V., Becherini, F., Scarchilli, C., Ciardini, V., Carugati, G., and Frezzotti, M.: Snow Accumulation Rates at Concordia Station, Antarctica, Observed by Stake Farms, *EGU sphere*, pp. 1–26, <https://doi.org/10.5194/egusphere-2025-2477>, 2025.

- 685 Traversi, R., Becagli, S., Castellano, E., Cerri, O., Morganti, A., Severi, M., and Udisti, R.: Study of Dome C Site (East Antarctica) Variability by Comparing Chemical Stratigraphies, *Microchemical Journal*, 92, 7–14, <https://doi.org/10.1016/j.microc.2008.08.007>, 2009.
- van Wessem, J. M., van de Berg, W. J., Noël, B. P. Y., van Meijgaard, E., Amory, C., Birnbaum, G., Jakobs, C. L., Krüger, K., Lenaerts, J. T. M., Lhermitte, S., Ligtenberg, S. R. M., Medley, B., Reijmer, C. H., van Tricht, K., Trusel, L. D., van Ulf, L. H., Wouters, B., Wuite, J., and van den Broeke, M. R.: Modelling the Climate and Surface Mass Balance of Polar Ice Sheets Using RACMO2 – Part 2: Antarctica
690 (1979–2016), *The Cryosphere*, 12, 1479–1498, <https://doi.org/10.5194/tc-12-1479-2018>, 2018.
- Wagnon, P., Delmas, R. J., and Legrand, M.: Loss of Volatile Acid Species from Upper Firn Layers at Vostok, Antarctica, *Journal of Geophysical Research: Atmospheres*, 104, 3423–3431, <https://doi.org/10.1029/98JD02855>, 1999.
- Wang, X., Langen, P. L., Li, R., Qiao, G., Fan, X., Dou, Y., and Cui, X.: Comparing Surface Mass Balance and Surface Temperatures From Regional Climate Models and Reanalyses to Observations Over the Antarctic Ice Sheet, *International Journal of Climatology*, 45, e8767,
695 <https://doi.org/10.1002/joc.8767>, 2025.
- Wang, Y., Ding, M., van Wessem, J. M., Schlosser, E., Altnau, S., van den Broeke, M. R., Lenaerts, J. T. M., Thomas, E. R., Isaksson, E., Wang, J., and Sun, W.: A Comparison of Antarctic Ice Sheet Surface Mass Balance from Atmospheric Climate Models and In Situ Observations, *Journal of Climate*, 29, 5317–5337, <https://doi.org/10.1175/JCLI-D-15-0642.1>, 2016.
- Zuhr, A. M., Münch, T., Steen-Larsen, H. C., Hörhold, M., and Laepple, T.: Local-Scale Deposition of Surface Snow on the Greenland Ice
700 Sheet, *The Cryosphere*, 15, 4873–4900, <https://doi.org/10.5194/tc-15-4873-2021>, 2021.

SUPPLEMENTARY MATERIAL TO:

Inter-annual snow accumulation and meter-scale variability from trench measurements at Dome C, Antarctica

Adrien Ooms¹, Mathieu Casado¹, Ghislain Picard², Laurent Arnaud², Maria Hörhold³, Andrea Spolaor⁴, Rita Traversi⁴, Joel Savarino², Patrick Gino², Pete Akers⁵, Birthe Twarloh³, and Valérie Masson-Delmotte¹

5 1 Laboratoire des Sciences du Climat et de l'Environnement, LSCE/IPSL, CEA-CNRS-UVSQ, Université Paris-Saclay, Gif sur Yvette, France

2 Institut des Geosciences de l'Environnement (IGE), Université Grenoble Alpes / CNRS, UMR 5001, Grenoble, France

3 Department of Geosciences, Alfred-Wegener-Institut Helmholtz-Zentrum für Polar- und Meeresforschung, Bremerhaven, Germany

10 4 Institute of Polar Sciences, National Research Council of Italy (ISP-CNR), Venice, Italy

5 Discipline of Geography, School of Natural Sciences, Trinity College Dublin, Dublin, Ireland

Correspondence: Adrien Ooms (adrien.ooms@lsce.ipsl.fr) and Mathieu Casado (mathieu.casado@lsce.ipsl.fr)

Contents of this file

Supplementary text S1 to S7

15 Figures S1 to S8

Appendix S

S1 Details on SSA analysis

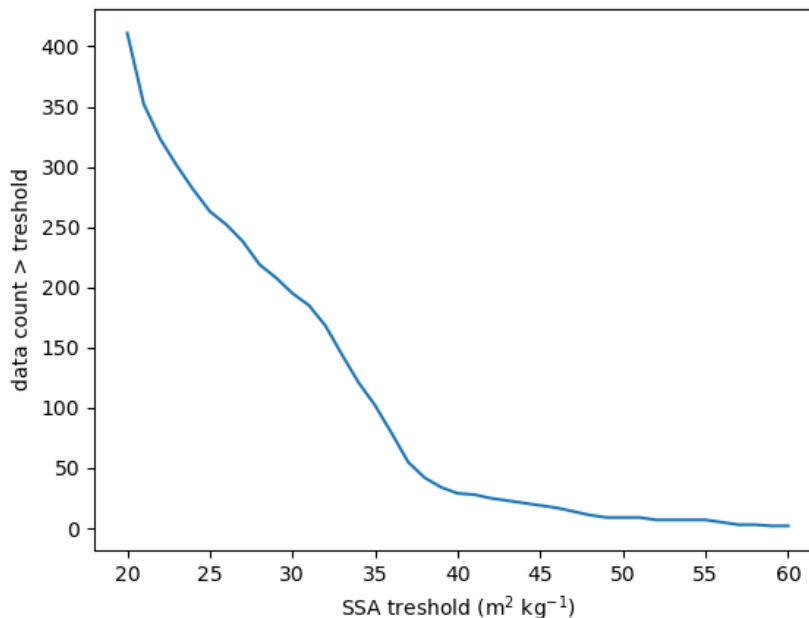


Figure S1. We have performed a sensitivity test to ensure that this was also an appropriate threshold for the trench dataset. We counted all SSA values in the trench dataset (26 evenly distributed profiles) above a certain threshold, for threshold values ranging from 20 m²kg⁻¹ to 60 m²kg⁻¹. We see a clear transition around 38-42 m²kg⁻¹, where the datapoint count increases sharply under 38 m²kg⁻¹, indicating a longer persistence of such SSA values during grain coarsening. This confirms that 40 m²kg⁻¹ is a sweet spot to identify fresher snow.

SSA. In our alignment protocols, we have only used SSA to get the topmost tie point for each profile in the upper section of the trench. SSA values exhibit a steady decrease in the first 40 cm just under the surface. Surface SSA can be as high as 70 m²kg⁻¹ in the surface layers and drop consistently below 20 m²kg⁻¹ at 40 cm depth and beyond.

It has been already documented that SSA values of 60 m²kg⁻¹ and above correspond to snow from the winter season (Picard et al., 2016b). In our case, high SSA value can only correspond to snow from the 2019 winter season. It is not expected for SSA slopes to align as a direct result of the sulfate isochrone alignment. Indeed, grain size growth depends on the burial history of the snow. Snow that has been exposed for a longer time will be subject to metamorphism for an extended period, resulting in a sharper gradient of SSA.

In (Fig. S2), SSA data show a sharp decrease across the 2020 to 2018 isochrones. The maximum value of SSA at the 2019 level is 37 m² kg⁻¹, and the 90% quantile is 35 m²kg⁻¹. So values of SSA under 37 m² kg⁻¹ at the time of the trench

sampling on the East Antarctic plateau can be attributed to snow older than a year. Another argument for choosing this threshold comes from the distribution of SSA values across the trench (Fig. S1). It shows a clear transition around 38-42 m^2kg^{-1} ,
30 showing a longer persistence of SSA values under 38 m^2kg^{-1} during grain coarsening, confirming that 40 m^2kg^{-1} is a sweet spot for identifying fresh snowfall at Dome C. Based on the distribution of SSA in surface snow (2019 level), with a mean value of 37 m^2kg^{-1} (and a 90% quantile of 35 m^2kg^{-1}), we interpret the fraction of profiles with SSA under the threshold value of 37 m^2kg^{-1} (indicator of snow older than a year) as the annual hiatus probability at the surface at the time of sampling. We identify about 20% of the profiles (6 out of 26) with surface SSA under this threshold. When using the 90% quantile threshold
35 (35 m^2kg^{-1}), the annual hiatus estimate for year 2019 is reduced to about 10% (three out of 26 profiles), giving a 10-20% estimate of annual hiatus for the year 2019.

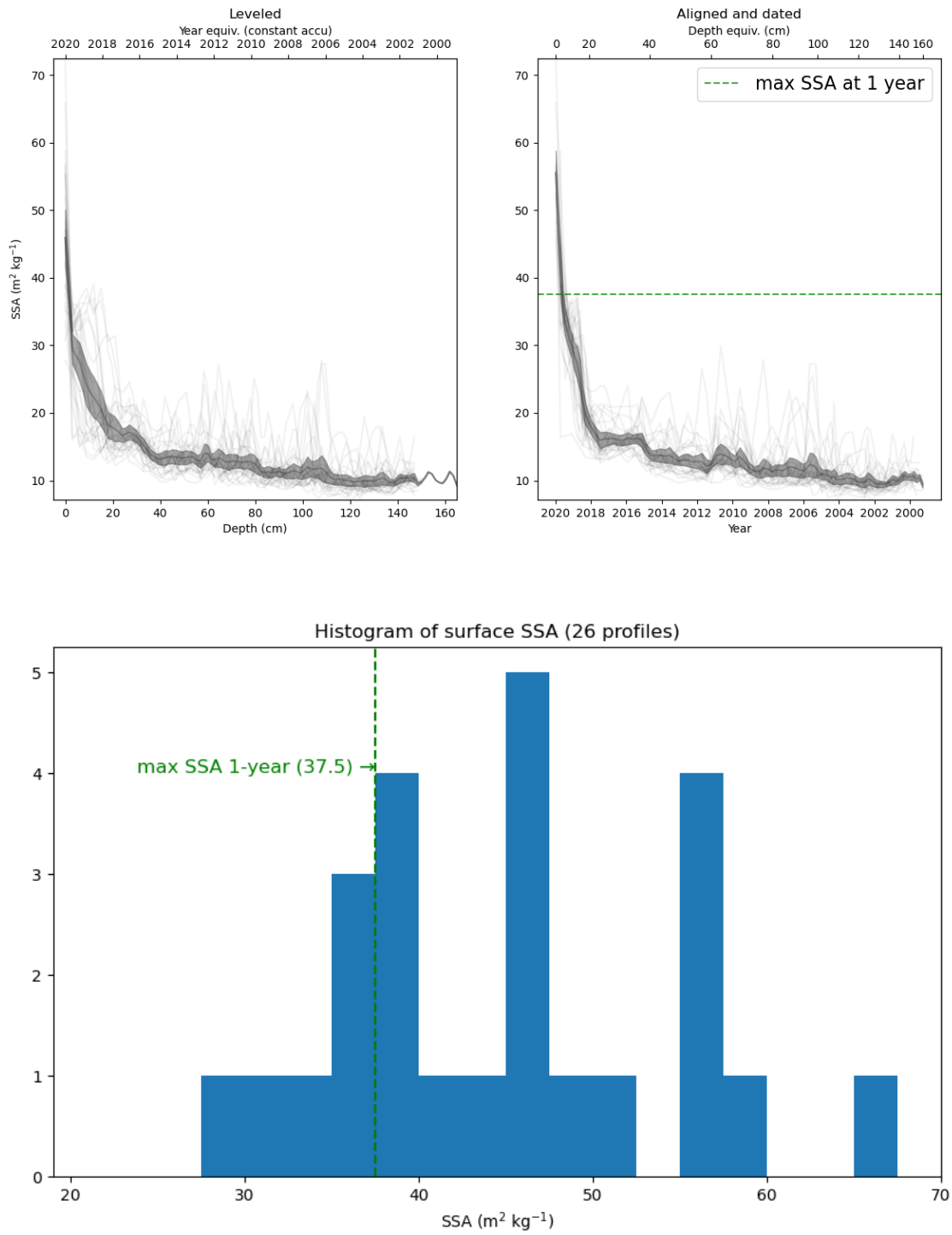


Figure S2. Decreasing behaviour with depth. 1 year SSA corresponds to the 35 unit threshold.

S2 Effect of the alignment on correlation patterns

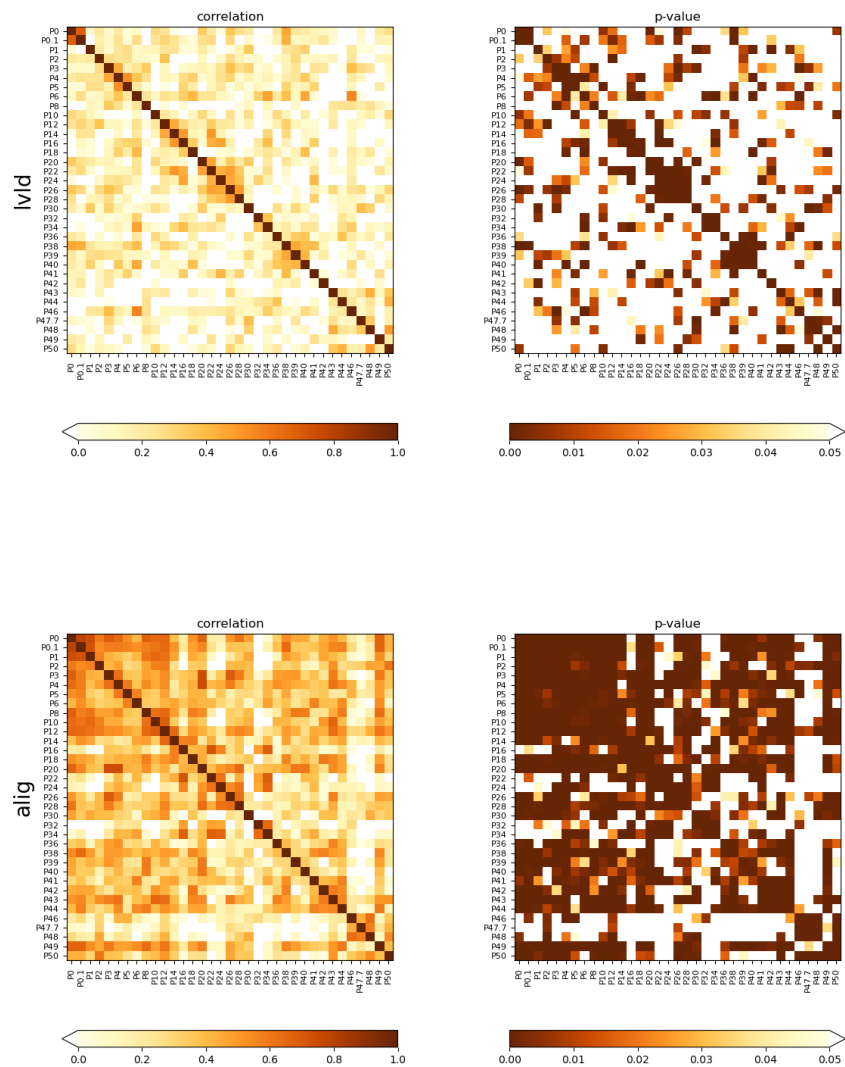


Figure S3. Quantitative diagnosis of the chemistry alignment described in section A3, showing a sharp increase in interprofile correlation across the entire trench after alignment. Only pits distant by 2 m have been used for mean correlation computation presented in the text.

S3 More details on the alignment

S3.1 Correcting for missing snow in the upper section of P0

40 In the results section, we explained how we chose P0 as reference profile for the alignment. P0 has a low value of SSA close to the surface, compared to most profiles in the trench, indicating a hiatus. A preliminary alignment of the highest SSA values across the trench indicates that 70% of profiles have 3 cm more snow (one data-point) than P0. If we used the raw depth scale of P0 with our protocol, we would be discarding this top snow layer, which would hinder the accumulation reconstruction for the top section of the trench. Instead, we proceed to extend the reference profile, adding two datapoint (3 cm at 1.5 cm
45 resolution) to the chemistry profiles of P0. We create a new reference profile for all species by filling these two data points with the average top 3 cm data of the other profiles with higher SSA values. This way, we obtain a reference profile on which an accurate alignment of the top section of the trench is possible.

S4 Sensitivity tests

S4.1 Using P48 as a reference profile

50 We redo the entire alignment and dating procedure starting from another profile P48 (the other 1.5 cm resolution profile in our dataset). The pair P0-P48 is a great example as it illustrates the differences that can exist between two profiles over the same depth range; they are shown in Figure S4: for example, a large peak around 35-40 cm depth in P0, which is also present in several profiles in the trench, is absent from P48. We recall that P48 sits on top of a dune and the other end of the trench, which could explain the differences in signal archival. This raises the question of how much the aligned trenches resulting from one
55 or another choice of reference can differ.

To illustrate this, we show the dated profiles P0 and P48 resulting from both alignments (Fig. S4). We get mismatches of up to a year in the position of the peaks. Here we have two factors at play; one is the way both profiles are aligned onto each other, which ought to be symmetric if our alignment is consistent; the second is the way each profile is dated in their respective alignment, which will depend on the matching features between our set of snow pits and the reference profile. When we look
60 at other profiles, discrepancies can amplify because of different choices in associating peaks to the reference. Comparing both alignments across the trench, the mean absolute difference in dates for each depth is 300 days for the entire trench, versus 150 days for P0 and P48.

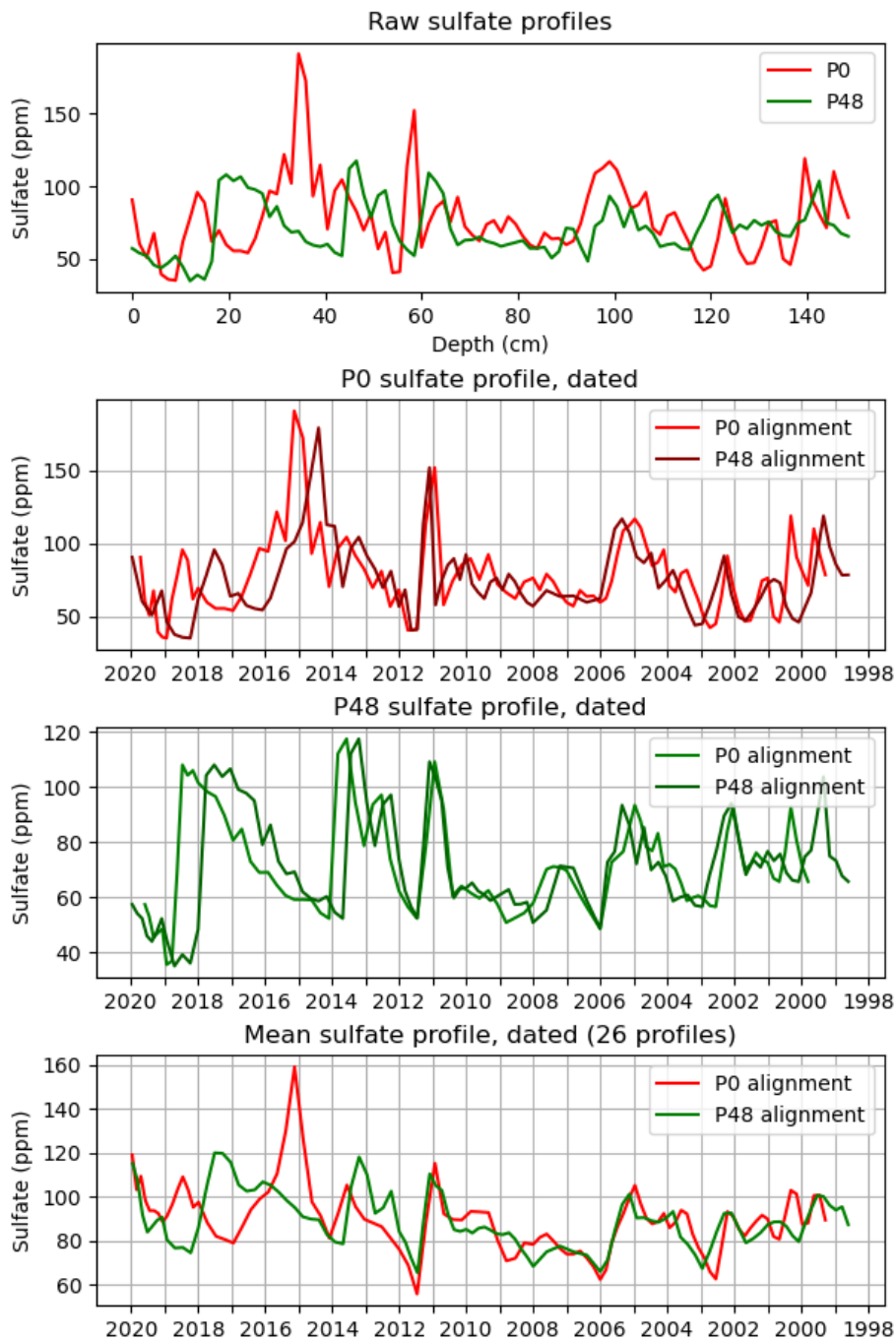


Figure S4. Sulfate profiles for P0 and P48 against depth and against time for alignment and dating procedures based on two different reference profiles.

Despite those differences, the mean accumulation reconstructions are extremely similar, as shown in Figure S5. The mean accumulation over the 20 year period is $23.9 \pm 1.5 \text{ kgm}^{-2}$ for the P0 alignment and $23.1 \pm 1.4 \text{ kgm}^{-2}$ for the P48 alignment
 65 ($\pm 1 \sigma$ spatial envelopes).

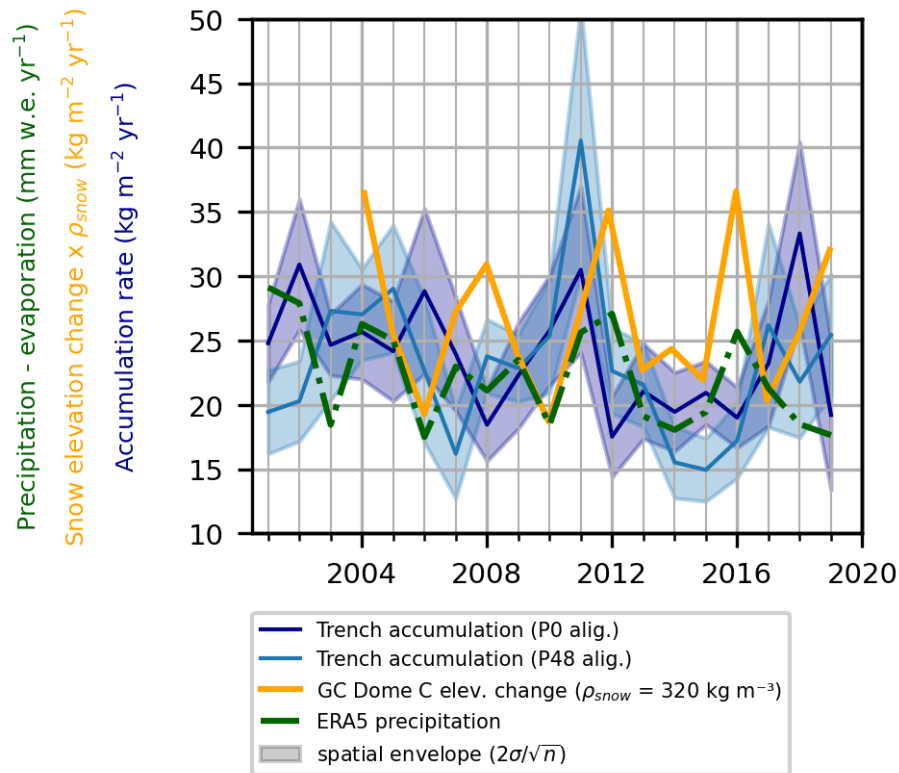


Figure S5. This figure illustrates the uncertainty arising from the choice of the reference profile: P0 as in the main text, or 48. We stress that, despite expected differences, as our method is not resolving annual variations, the two estimates lie within their spatial envelopes (shaded blue and purple curves), and the choice of the reference profile does not explain the differences between the trench and the GLACIOCLIM data.

S5 Snow accumulation distribution

The estimation of accumulation hiatus probability as presented in Section 3.4 relates to the more general question of the distribution of snow elevation change at a given time interval. Here we present two additional figures that illustrate how the trench dataset bridges between the two years of RLS high resolution snow elevation maps and the 14 years of GLACIOCLIM
 70 annual snow elevation change measurements. Fig. S6 (a) shows the distribution of snow accumulation rates, and Fig. S6 (b) shows the standard deviation.

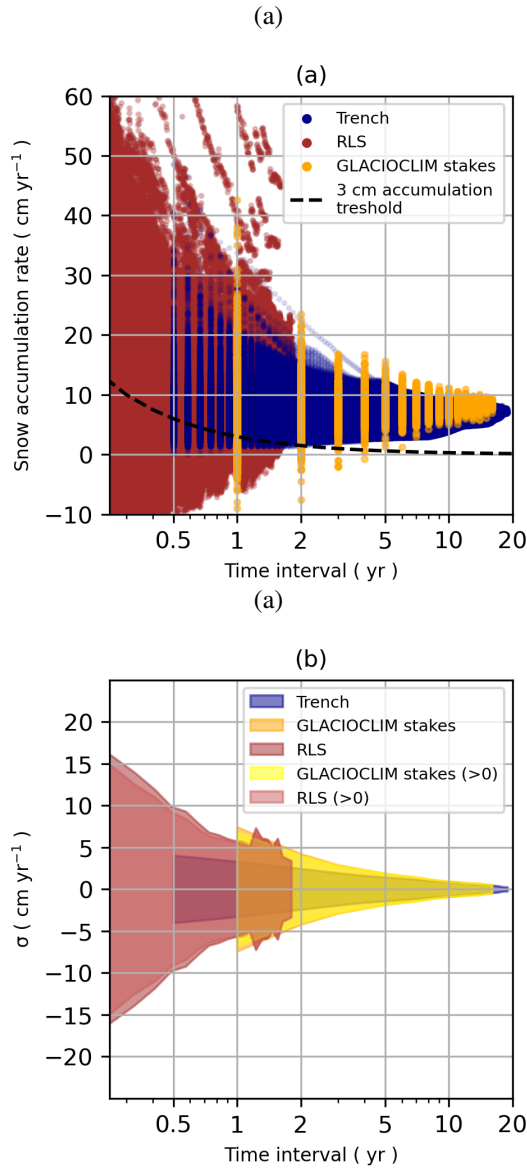


Figure S6. (a) Distribution of snow accumulation rate of single accumulation events according to the trench, RLS and GLACIOCLIM stakes datasets. Accumulation events are obtained from the datasets just as in Section 3.4, using daily elevation maps for RLS, monthly isochrones for the trench and yearly elevation readings for GLACIOCLIM. Time intervals under six months are discarded for the trench as they are under our resolution limit. This is an intermediate figure for the computation of hiatus probability: the black dashed line represents 3 cm total accumulation which is the threshold value for non-negligible snow accumulation. The hiatus probability for a given time period, as computed in Section 3.4, is the fraction of accumulation events under this threshold. (b) Standard deviation of accumulation rates over a given time interval for the trench, RLS and GLACIOCLIM stakes datasets. Same as (a) but centered around mean and given in standard deviation. The accumulation converges around the mean (mean/sigma < 1%) for periods longer than 10 years.

S6 Additional datasets

When comparing our accumulation estimates from the trench to ERA5 reanalysis data, one can ask whether another reanalysis dataset provides a better match, especially in terms of inter-annual variability and dephasing. We tested this with the Modern-Era Retrospective analysis for Research and Applications, version 2 (MERRA2) (Gelaro et al., 2017). We consider the grid-point closest to Dome C ($75^{\circ} 00' S$, $123^{\circ} 125' E$). The precipitation time series of MERRA2 along with the datasets of the main text is shown in Figure S7. The precipitation time series is very similar to ERA5, showing the same dephasing of annual precipitation peaks when compared to the trench accumulation time series. Note that we did not check the contribution of sublimation.

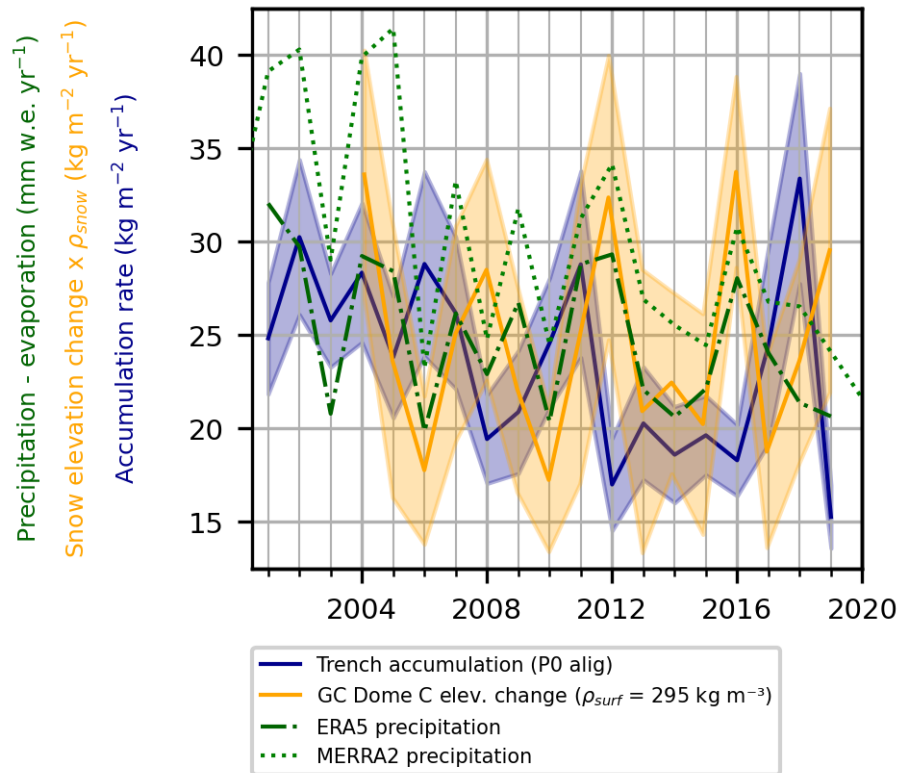


Figure S7. Same as figure 6 using MERRA2 in addition to ERA5 reanalysis precipitation outputs. MERRA2 and ERA5 precipitation datasets show a systematic offset and a quite close correlation that does not change the results. Note that here we show precipitation (as opposed to precipitation - sublimation in main text).

80 S7 Effect of the alignment on other chemical species

The isochrones presented in the results section are mainly based on the sulfate peak matching. It is interesting to check whether an increase in inter profile correlation of the signal is also visible on other chemical species in the aligned trench, compared to the raw data.

S7.1 MSA

85 MSA profiles shows a large inter-annual variability in the first 1 m under the surface, with three peaks above 25 ng g^{-1} , against a background value of $10\text{-}15 \text{ ng g}^{-1}$. Beyond 1 m depth, the signal is noticeably damped, with values around 10 ng g^{-1} in the 100-160 cm depth range.

After alignment, which we recall is mainly based on sulfate peak to peak matching, and only secondarily based on MSA, the common signal in MSA is nevertheless well improved. Inter profile correlation goes from 0.23 to 0.34 compared to the
90 leveled trench, and the number of significant correlations goes from 60% to 70%. The mean signal in the aligned trench, shown on the right in figure S8, is noticeably sharper than in the leveled trench.

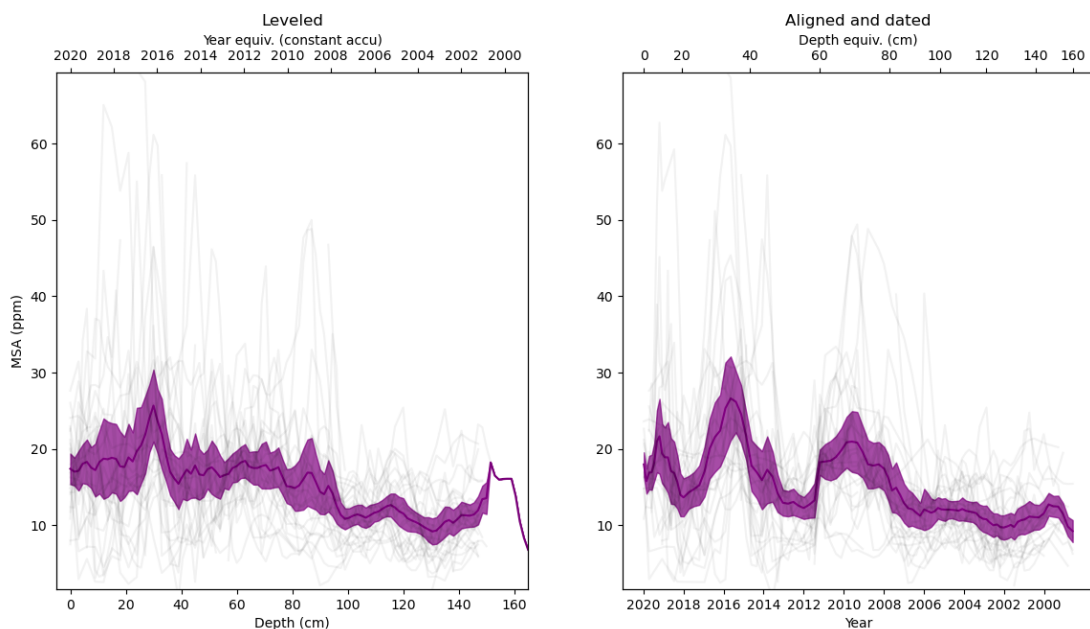


Figure S8. MSA profiles in the leveled and aligned trench, showing a damped signal below 1 m depth. Individual profiles are shown in light grey, and the purple curve represents the mean. The envelope indicates two standard deviation divided by \sqrt{n} .